BM@N Run6 Analysis Note v.3
Production of Λ hyperons in 4.0 AGeV and 4.5 AGeV carbon-nucleus interactions at the Nuclotron

Analysis team: M. Kapishin[1], A. Zinchenko[1], I. Rufanov[1], M. Zavertyaev[2], V. Vasendina[1], G. Pokatashkin, Yu. Stepanenko[1,3,*], K. Alishina[1]

[1] Joint Institute for Nuclear Research, Dubna, Moscow region, 141980, Russia
[2] Lebedev Physical Institute of the Russian Academy of Sciences, Moscow, 119991, Russia
[3] Gomel State University, Gomel, 246019, Belarus
*e - mail: yystepanenko@gmail.com

for BM@N Collaboration
April 2025

Abstract

Production of Λ hyperons in interactions of the carbon beam with the kinetic energy 4.0AGeV and 4.5 AGeV with the *C, Al, Cu, Pb* targets was studied with the BM@M detector at the Nuclotron. The analysis procedure is described in details. Results on Λ hyperons yields have been obtained and compared with the model predictions and another experiments.

BM@N configuration in the carbon beam run

The technical run of the BM@N detector was performed with the carbon beam in March 2017. The view of the BM@N setup used in the run is presented in Fig. 1 (left). The configuration of the central tracker was based on one plane of a forward silicon detector and six GEM stations combined from 5 GEM detectors with the size of 66x41 cm^2 and 2 GEM detectors with the size of 163x45 cm^2 [1]. More detailed configuration of the GEM detectors described in [2]. The tracking stations were arranged to have the beam passing through their centers (Fig. 1). Each successive GEM station was rotated by 180° around the vertical axis. It was done to have the opposite electron drift direction in the successive stations in order to avoid a systematic shift of reconstructed tracks due to the Lorentz angle in the magnetic field. The research program was devoted to measurements of inelastic reactions $C+A\rightarrow X$ with the beam kinetic energy of 4.0AGeV and 4.5AGeV and different targets: *C, Al, Cu, Pb*. The technical program of the run included the measurement of the carbon beam momentum in the central and outer tracker at different values of the magnetic field. Since the GEM tracker configuration was tuned to measure relatively high-momentum beam particles, the geometric acceptance for relatively soft decay products of strange *V0* particles was rather low.

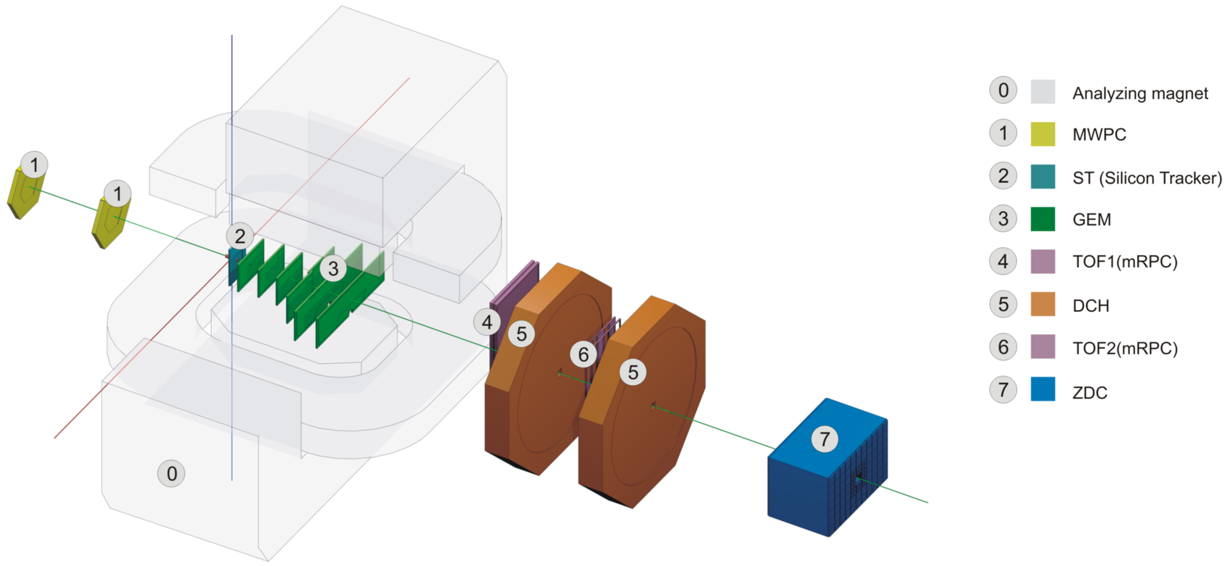

Figure 1. BM@N set-up in the carbon beam run (Run6)

In the present analysis the experimental data from the forward silicon detector, GEM detectors, trigger barrel multiplicity detector, beam, veto and T0 counters were used. The positions of the beam counters and trigger barrel detector and the target are given in Fig.2. The carbon beam intensity was few 10^5 per the spill, the spill duration was 2-2.5 sec. The magnetic field in the center of the analyzing magnet was 0.61 T.

Monte-Carlo simulation and event reconstruction

The Monte-Carlo (MC) event samples of $C+A$ collisions were produced with the DCM-QGSM event generator. The passage of particles through the setup volume was simulated with the GEANT4 program integrated into the BmnRoot software framework. To properly describe the GEM detector response in the magnetic field the microsimulation package Garfield++ was used.

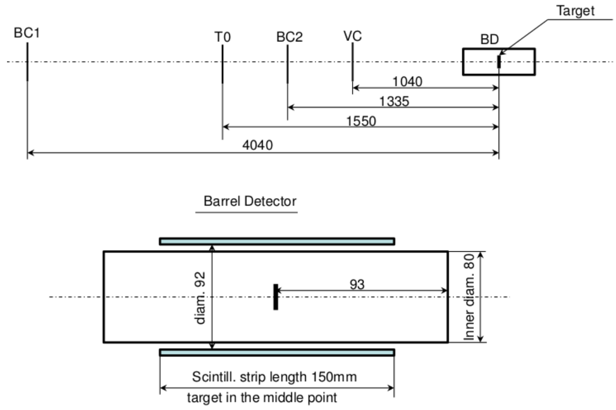

Figure 2. Schematic view and positions of the beam counters, barrel detector and target.

The package gives detailed description of the processes inside the GEM detector, including the drift and diffusion of released electrons in electric and magnetic fields and the electron multiplication in GEM foils, so that the output signal from the readout plane can be reproduced. To speed up the simulation, dependencies of the Lorentz shifts and the charge distributions on the readout planes on the drift distance were parameterized and used in the GEM digitization part of the BmnRoot package. The details of the detector alignment, Lorenz shift corrections are described in the paper [3]. The track reconstruction method was based on the so-called "cellular automaton" approach [4]. The tracks found were used to reconstruct primary and secondary vertices using the "KF-particle" formalism [5].

Track selection criteria

The total number of the statistics involved to the analysis was ~2.9×10^7 for the physical data and ~3.8×10^7 for Monte-Carlo simulation (for each target and energy). The Λ hyperons events candidates were reconstructed using their decay mode into two oppositely-charged tracks. Since particle identification was not used in the analysis, all positive tracks were considered as protons and all negative as π^-.

The tracks selection criteria were:

1. Number of tracks in selected events: positive >= 1, negative >= 1;
2. Beam halo, pile-up suppression within the readout time window: number of signals in the start detector: T0 = 1, number of signals in the beam counter: BC2 = 1, number of signals in the veto counter around the beam: Veto = 0;
3. Trigger condition in the barrel detector: number of signals BD >= 2 or BD >= 3 (energy and target dependent);

Table 1. ε_{pileup} suppression factors.

Selection	4 AGeV	4.5 AGeV
T0==1	+	+
BC2==1	+	+
Veto==0	+	+
C	0.674±0.034	0.529±0.026
Al	0.740±0.037	0.618±0.031

Cu	0.779±0.039	0.621±0.031
Pb	0.784±0.039	0.686±0.034

The suppression factors of reconstructed events ε_{pileup} due to selection criteria 2 applied to suppress beam halo and pile-up events in interactions of the 4.0 AGeV and 4.5 AGeV carbon beam with the *C, Al, Cu, Pb* targets are given in Table 1. The total number of triggered events, the beam fluxes and luminosities are summarized in Table 2.

Table 2. Number of triggered events, beam fluxes and integrated luminosities collected in interactions of the carbon beam of 4.0 and 4.5AGeV with different targets.

Interactions, target thickness	Number of triggers / 10^6	Integrated beam flux / 10^7	Integrated luminosity / 10^{30} cm^{-2}
4 AGeV, *C+C* (9 mm)	4.04	6.07	6.06
4 AGeV, *C+Al* (12 mm)	4.61	3.31	2.39
4 AGeV, *C+Cu* (5 mm)	4.87	4.71	2.00
4 AGeV, *C+Pb* (10 mm)	0.81	0.67	0.22

Interactions, target thickness	Number of triggers / 10^6	Integrated beam flux / 10^7	Integrated luminosity / 10^{30} cm^{-2}
4.5 AGeV, *C+C* (9 mm)	3.01	4.70	4.69
4,5 AGeV, *C+Al* (12 mm)	3.69	4.98	3.60
4.5 AGeV, *C+Cu* (5 mm)	5.44	7.21	3.06
4.5 AGeV, *C+Pb* (10 mm)	2.40	2.58	0.84

Monte-Carlo tuning

1. Gem's Efficiency

The two-dimensional (X, Y) efficiency distributions for six GEM station were calculated for the experimental data to reproduce the detector effects in the MC track reconstruction.

For each station they were estimated using the following approach:

1. Divide detectors area into 180x45 cells (along X and Y coordinates correspondently);
2. Select good quality tracks with the number of hits per track (excluding the station under study) not less than *N*;
3. Check that track crosses the detector area, if yes, add one track to the denominator;
4. If there is a hit in the detector, which belongs to the track, add one track to the numerator;
5. Detector efficiency = sum of tracks in numerator / sum of tracks in denominator.

Simulated amplitude signals in the GEM detectors were modified according to amplitudes of the experimental signals in these detectors. GEM (*X, Y)* efficiencies for data and MC are presented in Fig. 3 and Fig. 4. One-dimensional comparison GEM efficiencies between the experimental data and MC shown in Fig. 5. Discrepancies between data and MC do not exceed 10% range.

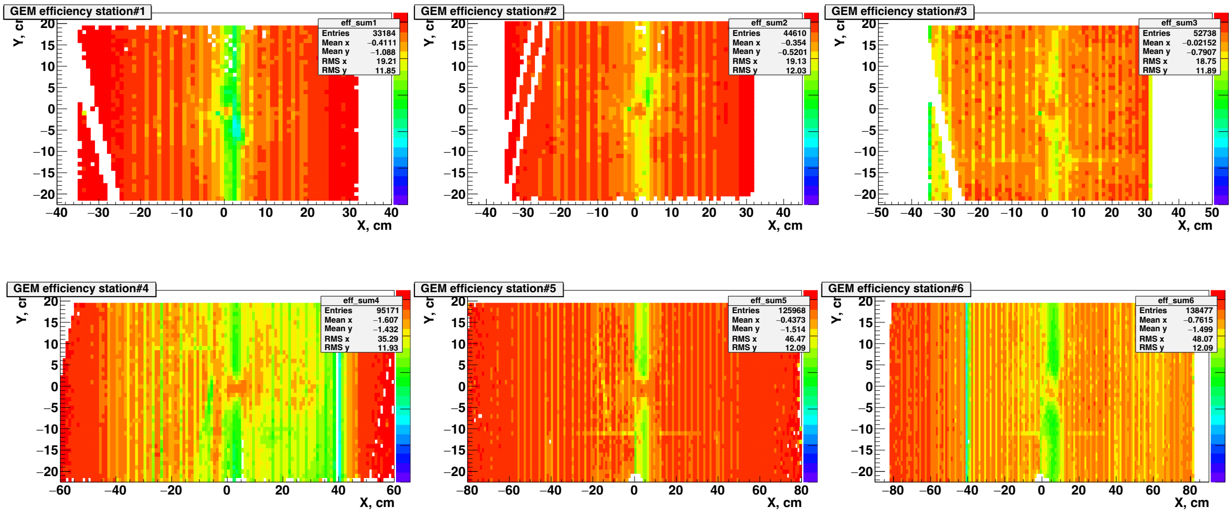

Figure 3. Two-dimensional *(X, Y)* efficiency distributions in six GEM stations measured with experimental tracks (C+C 4.0GeV process).

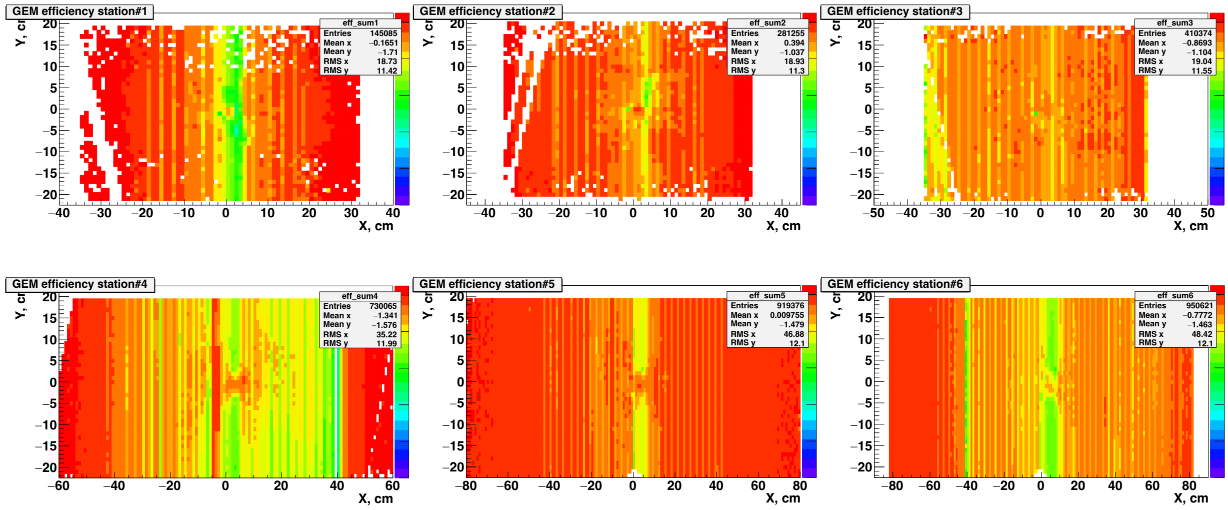

Figure 4. Two-dimensional *(X, Y)* efficiency distributions in six GEM stations implemented into Monte-Carlo simulation according to experimental data (C+C 4.0GeV process).

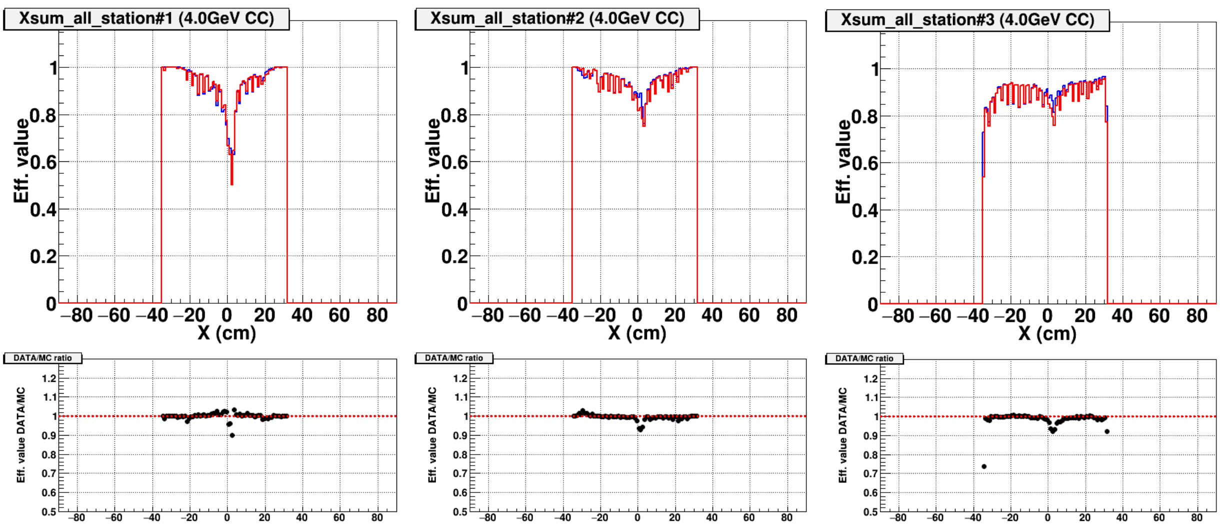

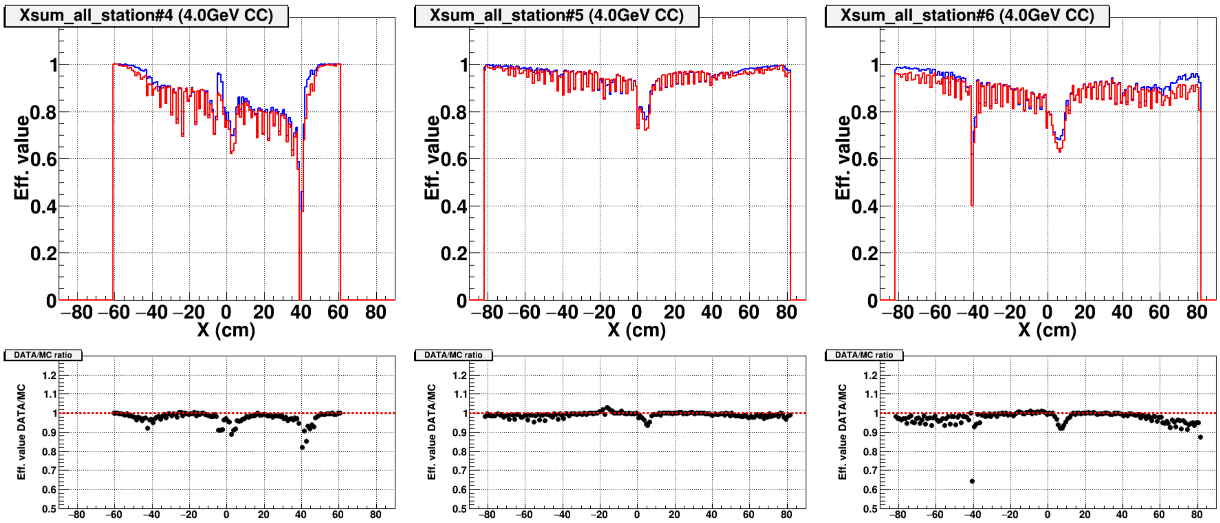

Figure 5. One-dimensional GEM efficiency comparison between the experimental data (red line) and MC (blue line). Pictures was obtained by integration along Y-axis. Black distributions correspond to the ratio of the data to MC distributions (C+C 4.0GeV process).

1. Track hits residual corrections

The dx -residual values and their corresponding errors were analyzed for each GEM station [6] for the MC samples and the physical data

The dx-residual value (and the same for dy-residual) corresponds to the difference between the x_{rec} hit coordinate of the reconstructed track and the x_{ext} hit coordinate of the extrapolated track in GEM station *z*-position. The x_{ext} value was calculated by excluding the reconstructed track hit from the considered GEM station and further extrapolation of this track to this GEM plane. The geometrical interpretation of the dx-residual is presented in Fig. 6, where $dx = (x_{rec} - x_{ext})$ is the value of dx-residual in considered GEM detector station.

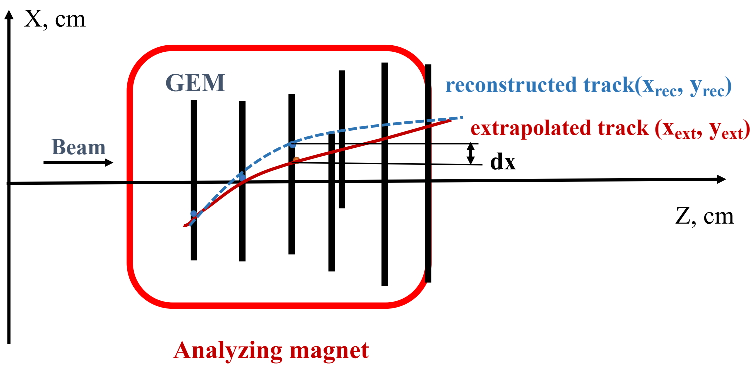

Figure 6. Geometrical definition of dx-residual value, where x_{rec} is reconstructed track x hit position and x_{ext} is extrapolated track x hit position in GEM station.

Tracks with at least four hits out of six in the central tracker (GEM detectors) were selected for the dx-residual analysis. The two-dimensional dependencies of the dx value versus x were calculated for each GEM station, where x corresponds to the extrapolated track hit coordinate (x_{ext}) in the detector plane Fig. 7. After that $dx(x)$ distributions were sliced along the x-axis for each GEM detector and one-dimensional dx-distributions were fitted using the sum of the second-order polynomial function and the Gaussian function (1) (Fig. 8):

$$F(dx)_{fit} = p_0 + p_1 dx + p_2 dx^2 + \; p_3 \exp\left(-\frac{1}{2}\left(\frac{dx-p_4}{p_5}\right)^2\right), \tag{1}$$

where: $p_0, \ldots p_5$ are free parameters of the fit function;
dx - is the value of the residual.

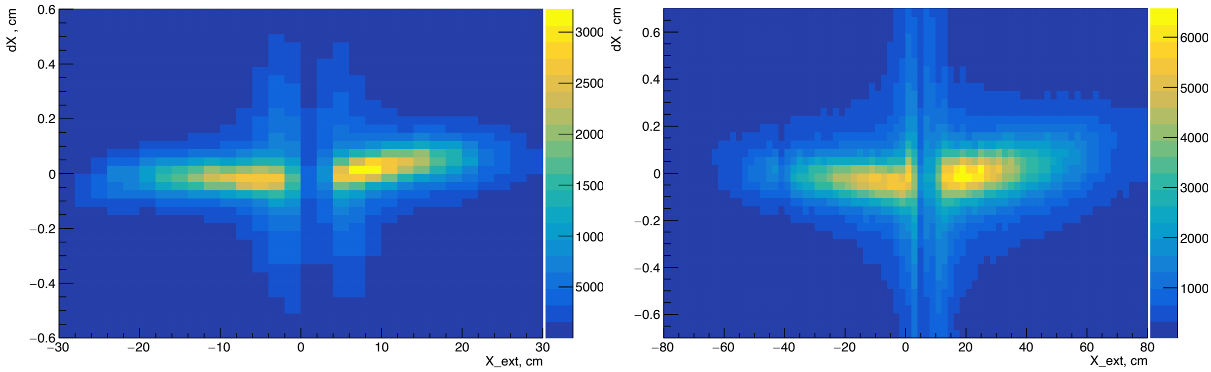

Figure 7. The two-dimensional $dx(x)$ distributions. *C*+*Cu* 4.0 AGeV data for 2nd (left) and 6th (right) stations.

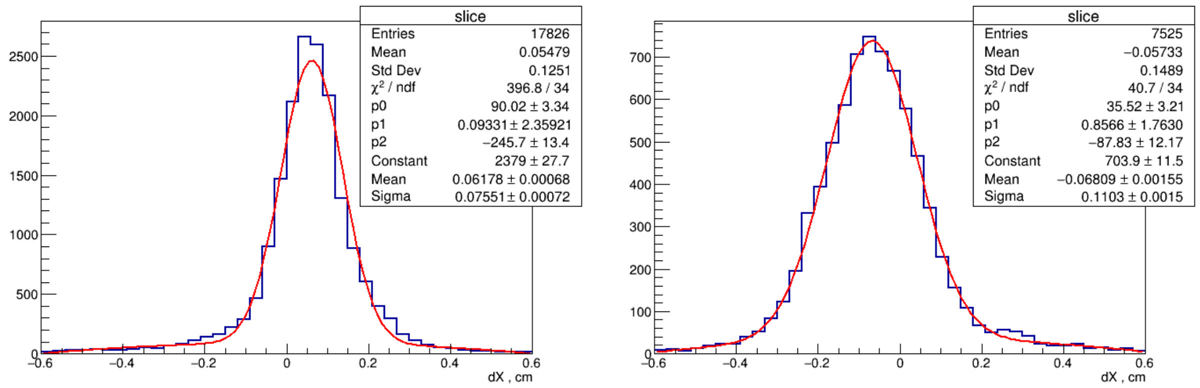

Figure 8. The one-dimensional sliced $dx(x)$ distributions with fit function (1.1). *C*+*Cu* 4.0 AGeV data, 2nd GEM station.

The values of the parameters p_4 (peak position of the Gaussian function) and p_5(width of the Gaussian function) which are correspond to the mean value position of the dx-residual and its determination error respectively were extracted from the fit. The distributions of the dx-residual mean position depending on the x coordinate for each GEM detector station are presented in blue square points in Fig. 9 and Fig. 10 for MC and data respectively.

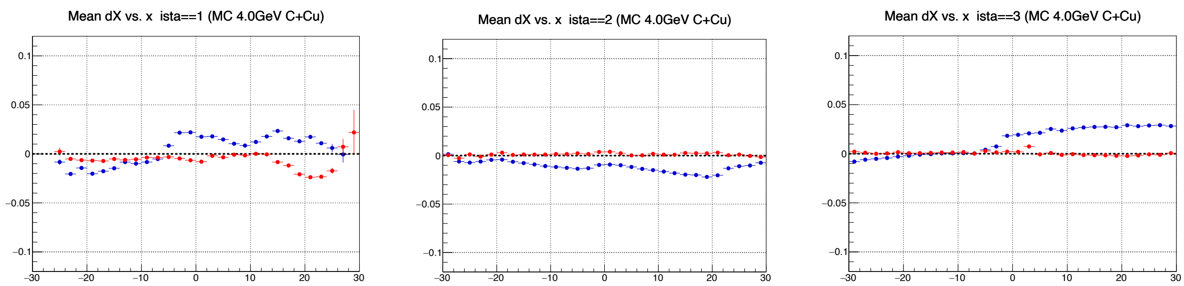

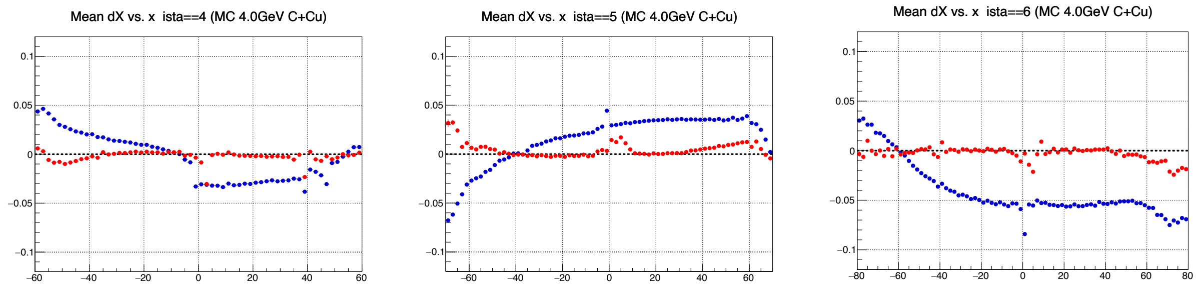

Figure 9. Mean dx-residuals vs. x for all GEM stations for MC. Blue square point to the mean dx-residuals before correction. Red triangle points to the mean dx-residuals after corrections. Reaction $C + Cu$, energy 4.0 GeV.

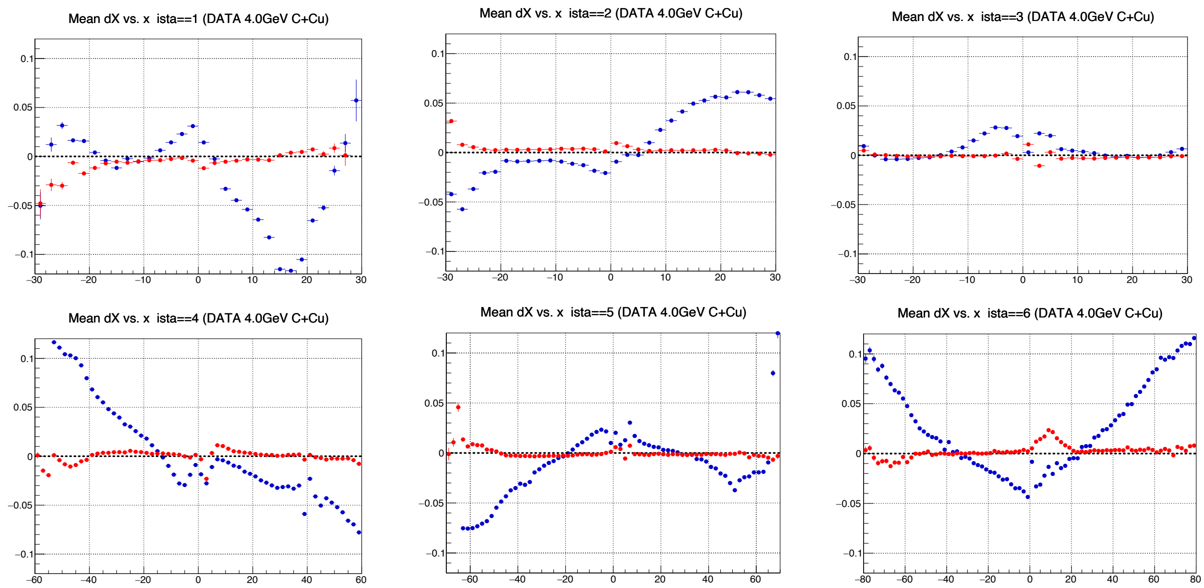

Figure 10. Mean dx-residuals vs. x for all GEM stations for experimental data. Blue square point to the mean dx-residuals before correction. Red triangle points to the mean dx-residuals after corrections. Reaction C+Cu, energy 4.0 GeV.

These distributions show that the position of the dx-residual mean values along the x-axis is not at zero positions; this suggest that the procedure of the track hits reconstruction in GEM detectors have discrepancies.

To improve the track hits reconstruction algorithm the iterative procedure of the dx-residual corrections was proposed and implemented. It consists of the following steps:

1. Calculate the dx-residual mean values depending on the x coordinate from the one-dimensional dx-distributions fits using (1) as described above;
2. Fit the $dx(x)$ distributions using two functions as (2) for positive and negative side of the detector along x coordinate;

$$F(x)_{fit} = p_0 + p_1x + p_2x^2 + p_3x^3 + p_4x^4 + p_5x^5, \tag{2}$$

where: $p_0, \ldots p_5$ are free parameters of the fit function;
x is coordinate of the track hit along the x-axis of the GEM station.

3. Make corrections of reconstructed x_{rec} values using functions (2) with extracted parameters from the fits (step 2) for positive and negative side of the detector along x coordinate: $x_{rec} = x_{rec} - 0.5 \cdot F(x)_{fit}$
4. Calculate new $dx(x)$ distributions (as in step 1);

5. Compare distributions before and after corrections;
6. Repeat dx-residual corrections procedure if necessary (steps 1-5).

The result of dx-residual corrections is presented in Figs. 9 and Fig. 10 in red points. It was obtained after applying dx-residual corrections algorithm two times. Distributions after corrections show that the accuracy of the reconstructed track hits coordinates (x_{rec}) in the GEM stations was improved as for data as for MC simulation.

The procedure of the track hit residual corrections was applied for all energies and targets in Run-6 analysis.

2. Track hit position error corrections

After applying the track hits position correction procedure, the hit deviations from the reconstructed track was evaluated using physical data and corresponding corrections were applied in MC (parameter p_5 from 1) The result of the corrections is shown in Fig. 11 for dx-residuals and in Fig.12 for dy-residuals.

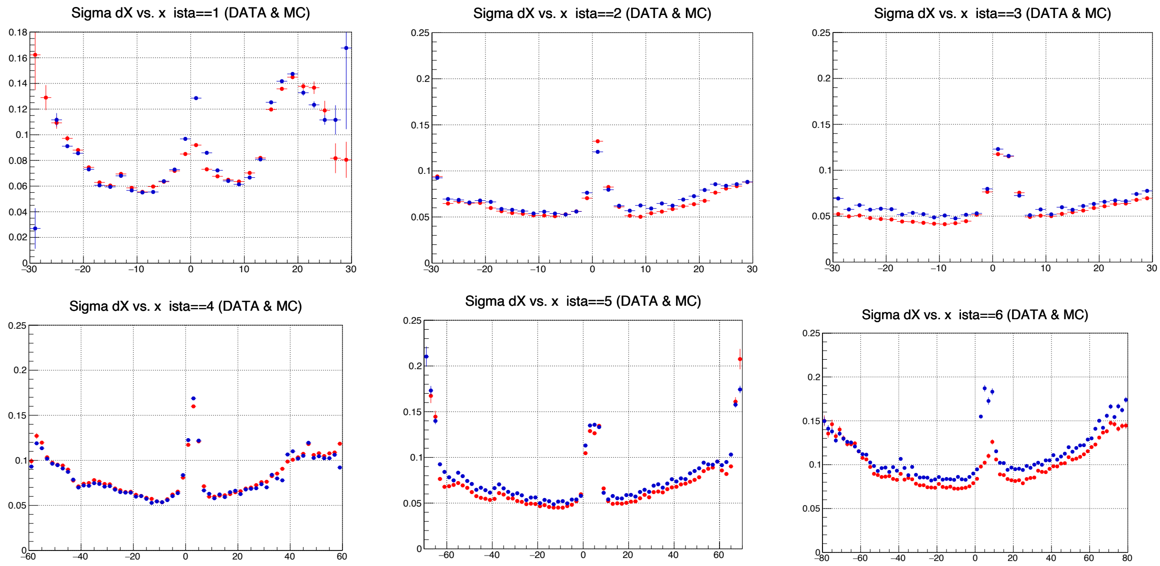

Figure 11. The error width of the dx-residuals determination vs. x for all GEM station after corrections. Blue points - MC, red points - data. Reaction *C+Cu*, energy 4.0 GeV.

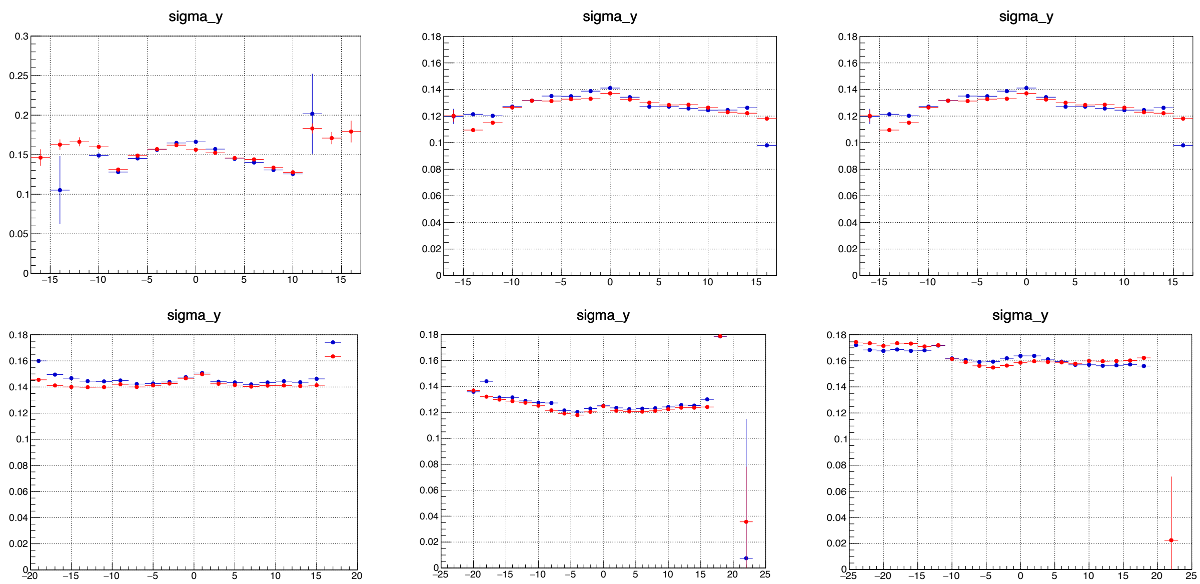

Figure 12. The errors width comparison of the dy-residuals determination vs. y for all GEM station. Blue points - MC, red points - data. Reaction $C + Cu$, energy 4.0 GeV.

3. Residuals width vs. momentum corrections

The dependence of the dx-value versus momentum of track for each GEM was calculated. From the fit function (1) the distribution of the parameter p_5 value (width of the Gaussian function) depending on the momentum of track for each GEM station was calculated for data and MC (Fig. 13).

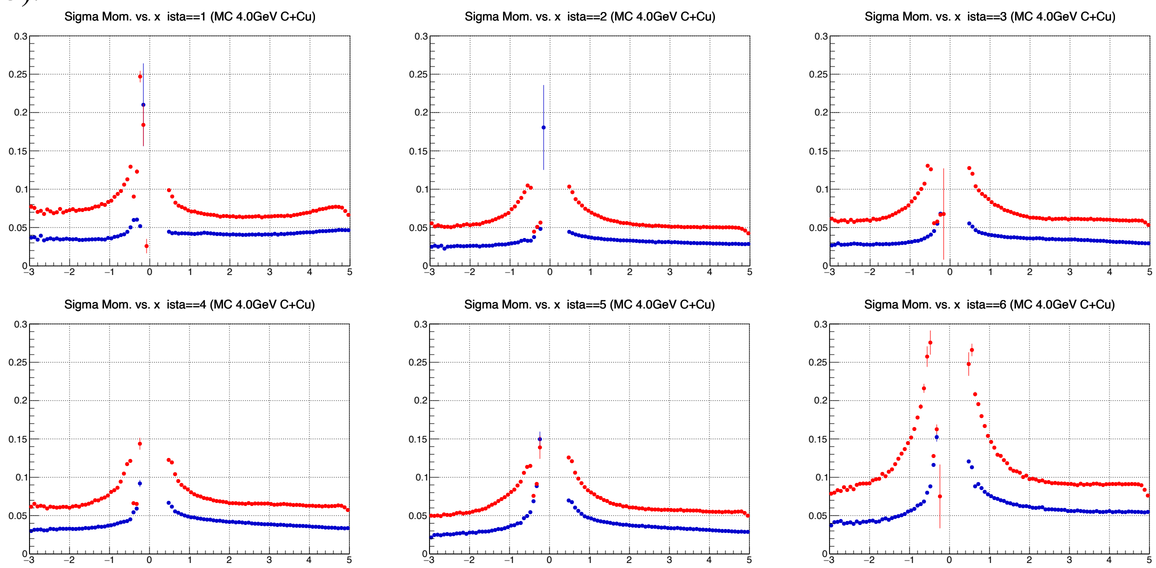

Figure 13. Dependencies residuals errors vs. track momentum for all GEM stations. Blue points - MC, red points - data. Reaction $C + Cu$, energy 4.0 GeV.

Using smearing function $\sigma_{smear} = \sqrt{\sigma_{data}^2 - \sigma_{MC}^2}$ residuals errors vs. track momentum distributions in MC were adjusted to the data (Fig. 14).

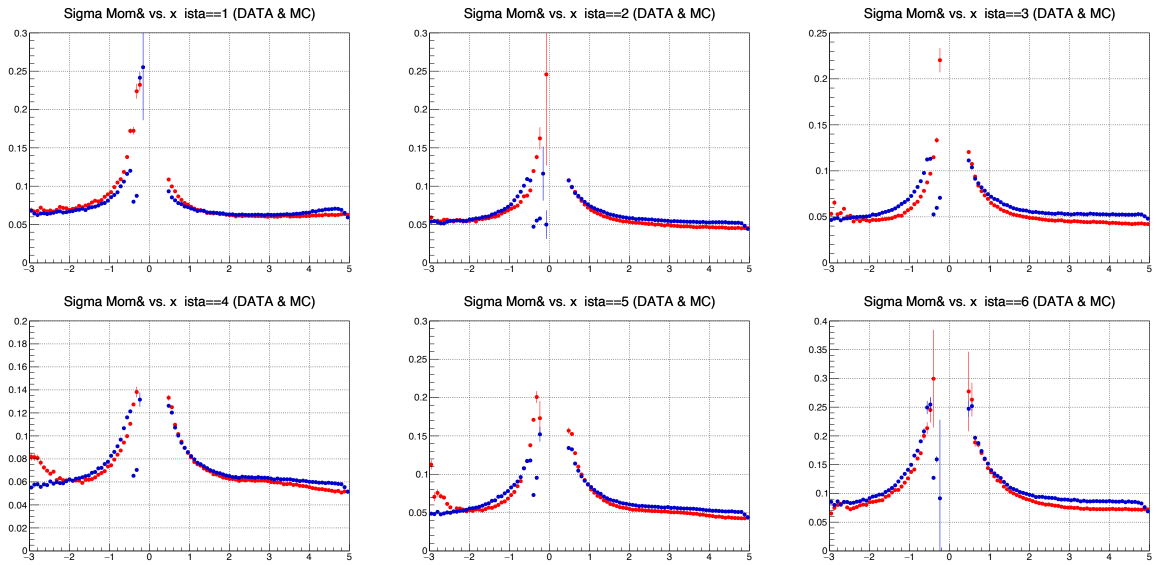

Figure 14. Dependencies residuals errors vs. track momentum for all GEM stations after smearing procedure. Blue points - MC, red points - data. Reaction C+Cu, energy 4.0 GeV.

Λ hyperon selection criteria

Λ hyperon is a long living particle ($\tau = (2.632 \pm 0.020) \times 10^{-10} s$) which is decaying with the highest probability into two channels: $\Lambda \rightarrow p\pi^-$ with $BR = (63.9 \pm 0.5)\%$ and $\Lambda \rightarrow n\pi^0$ with $BR = (35.9 \pm 0.5)\%$.

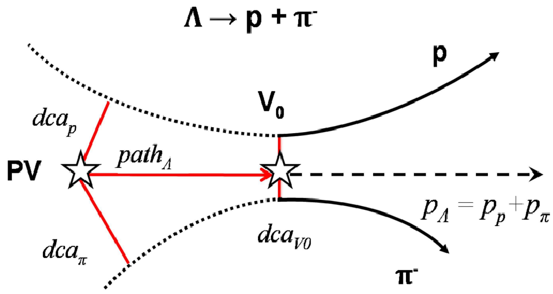

Figure. 15. Decay Scheme. Event topology: PV – primary vertex, V_0 – vertex of hyperon decay, dca – distance of the closest approach, path – decay length.

Λ hyperons were reconstructed using their decay mode into two oppositely-charged tracks $\Lambda \rightarrow p\pi^-$. The signal event topology (decay of a relatively long-lived particle into two tracks) defined the selection criteria: small track-to-track separation in the decay vertex, relatively large decay length of the mother particle (Fig. 15).

After the track selection procedure, the next cuts were applied for the Λ hyperon signal selection:

1. Each track has at least 4 hits in Si and GEM detectors (7 detectors in total), where hit is a combination of two strip clusters on both readout sides (X and X' views) on each detector [1];
2. Momentum range of positive tracks: p_{pos}< 3.9, 4.4 GeV/c for 4.0AGeV and 4.5 AGeV respectively;
3. Momentum range of negative tracks: p_{neg}> 0.3 GeV/c;
4. Distance of the closest approach of *V0* decay tracks (distance in X-Y plane between *V0* decay tracks at Z=Z_{V0}): *dca* < 1.0 cm;
5. Distance between *V0* and primary vertex: *path* > 2.5 cm.

Data and Monte-Carlo comparison

To evaluate the Λ hyperon acceptance and reconstruction efficiencies, minimum bias interactions of 4.0AGeV and 4.5AGeV carbon beam with *C, Al, Cu, Pb* targets were generated with the DCM-QGSM generator. Distributions of the experimental primary vertex are given in Fig.16. The generated particles were traced through the BM@N detector geometry using the GEANT4 simulation and reconstructed using the BmnRoot software framework. The total number of MC generated events for each target and energy is ~3.8×10^7.

Experimental and Monte-Carlo distributions of the reconstructed tracks number in the primary vertex and number of hits for positive and negative tracks are presented in Fig.17 and Fig.18 for 4.0AGeV and 4.5 AGeV carbon beam data, respectively. Distributions of the transverse momentum p_T and total momentum p of reconstructed positive and negative particles in data and MC simulation are shown in Fig. 19 and Fig. 20 for interactions of 4.0AGeV and 4.5AGeV carbon beam, respectively. Distributions of spatial parameters (*path* and *dca*) used for the Λ hyperon selection are presented in Fig.21 and Fig. 22. for 4.0AGeV and 4.5AGeV energies respectively.

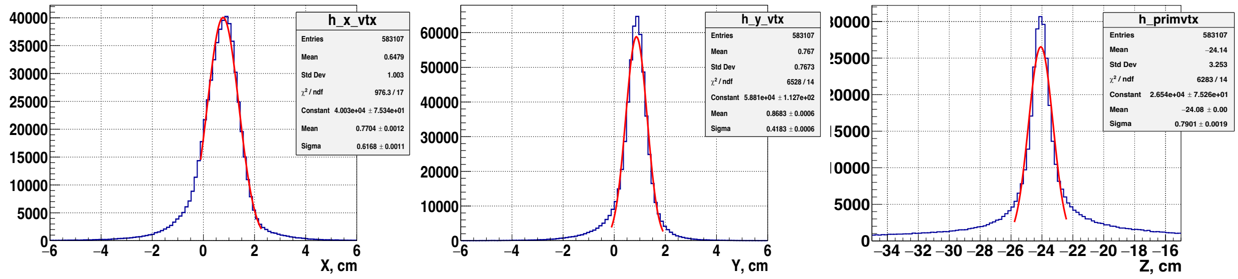

Figure. 16. *X,Y,Z* distributions of the experimental primary vertex

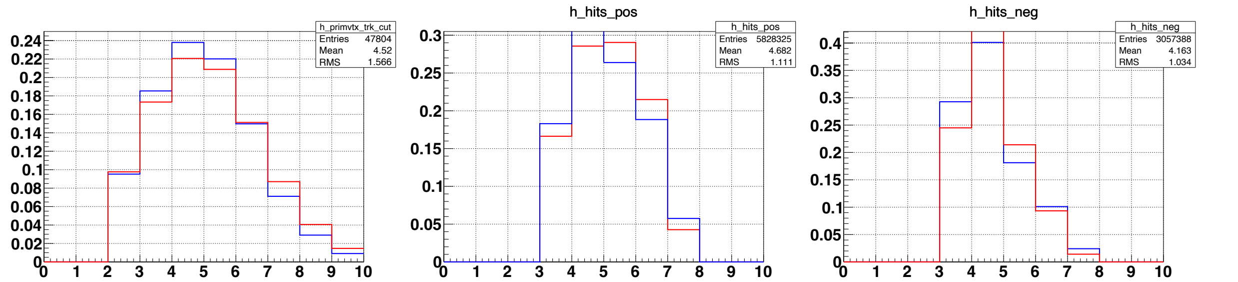

Figure. 17. *C+Cu* interactions at 4.0AGeV carbon beam energy: number of tracks reconstructed in the primary vertex (left); number of hits per reconstructed track for positive particle (center); number of hits per reconstructed track for negative particle (right). Blue points - MC, red points - data. (redraw)

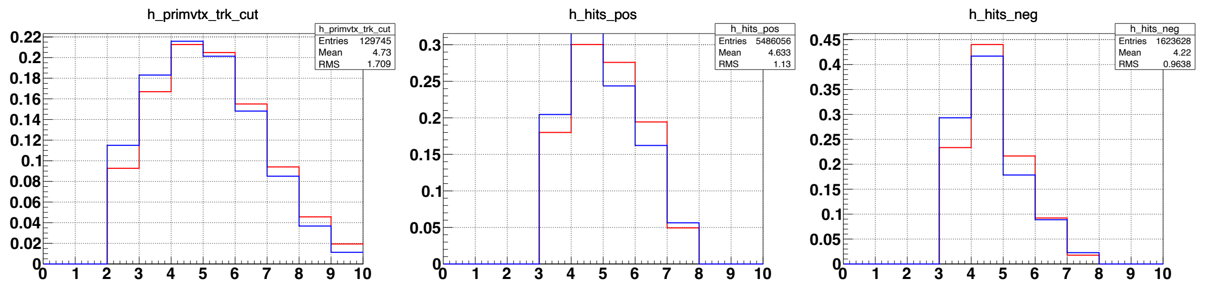

Figure. 18. *C+Cu* interactions at 4.5 AGeV carbon beam energy: number of tracks reconstructed in the primary vertex (left); number of hits per reconstructed track for positive particle (center); number of hits per reconstructed track for negative particle (right). Blue points - MC, red points - data. (redraw)

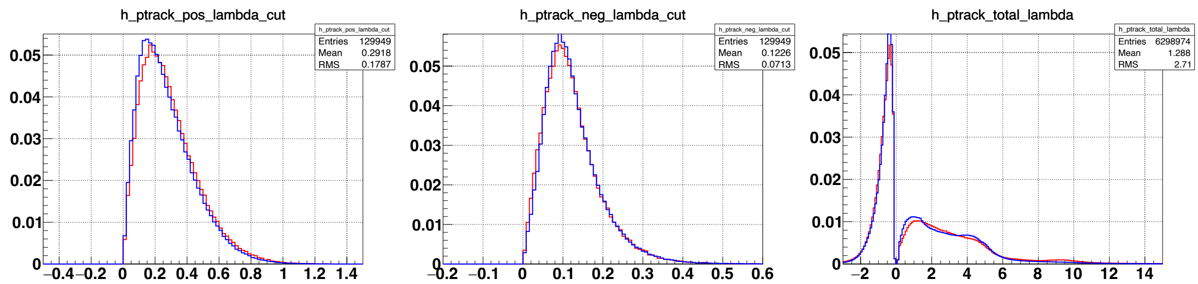

Figure 19. *C+Cu* interactions at 4.0AGeV carbon beam energy: transverse momentum of positive particles (left); transverse momentum of negative particles (center); total momentum of negative (p/q<0) and positive particles (p/q>0) (right). Blue points - MC, red points - data. (redraw)

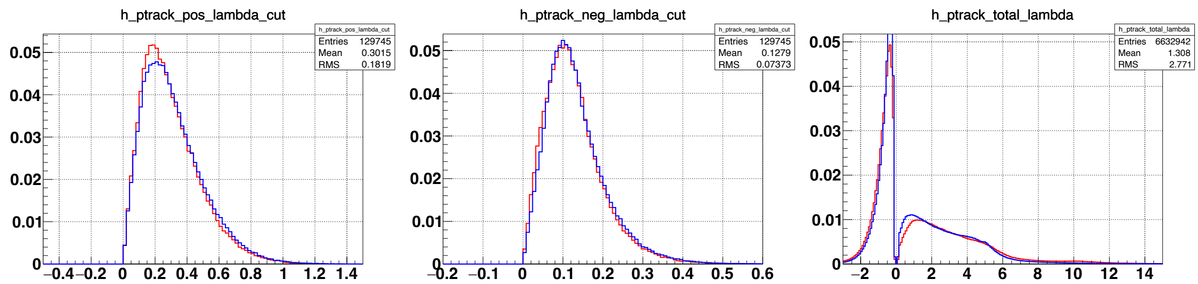

Figure 20. *C+Cu* interactions at 4.5 AGeV carbon beam energy: transverse momentum of positive particles (left); transverse momentum of negative particles (center); total momentum of negative (*p/q*<0) and positive particles (*p/q*>0) (right). Blue points - MC, red points - data. (redraw)

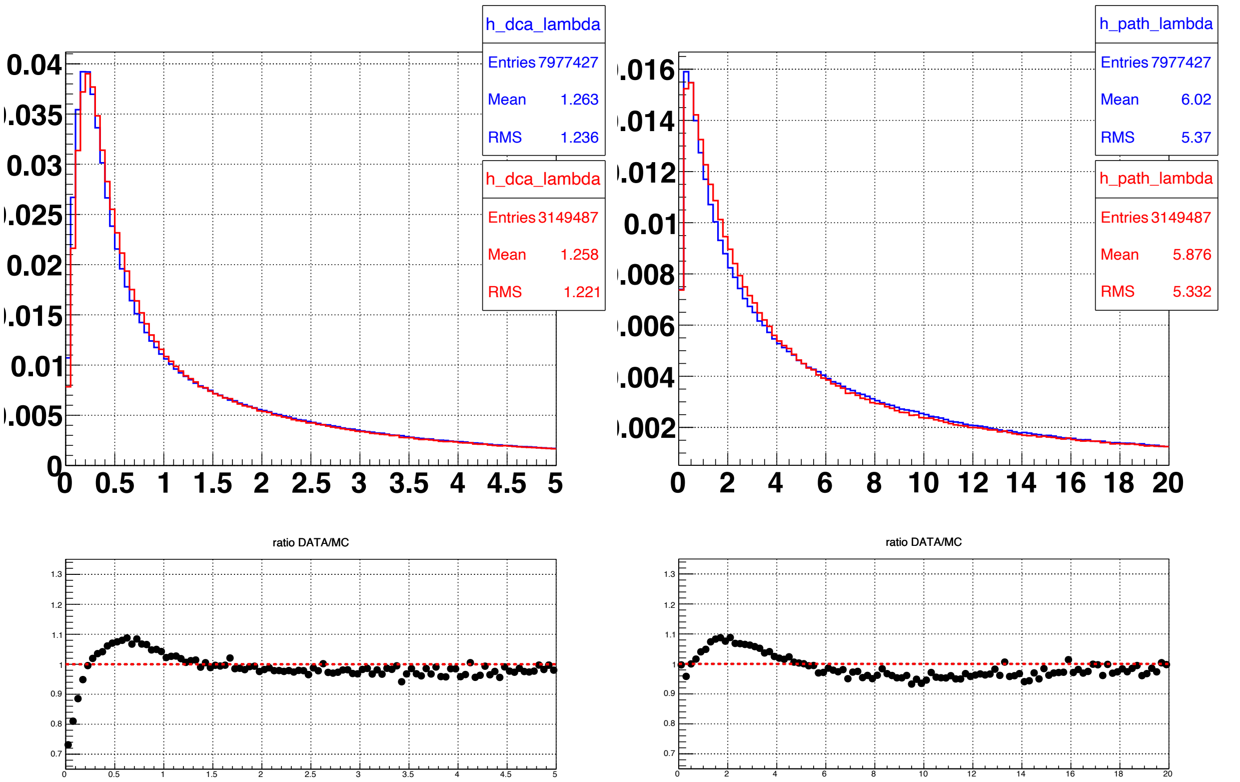

Figure 21. Distance of the closest approach of *V0* decay tracks (*dca*) (left plot) and distance between the primary vertex and *V0* (*path*) (right plot). Ratio of the data/MC presented on bottom pictures. Cuts were applied as follow: *dca<1.0, path>2.5*. Reaction *C+Cu*, energy 4.0 GeV. (redraw with x axis)

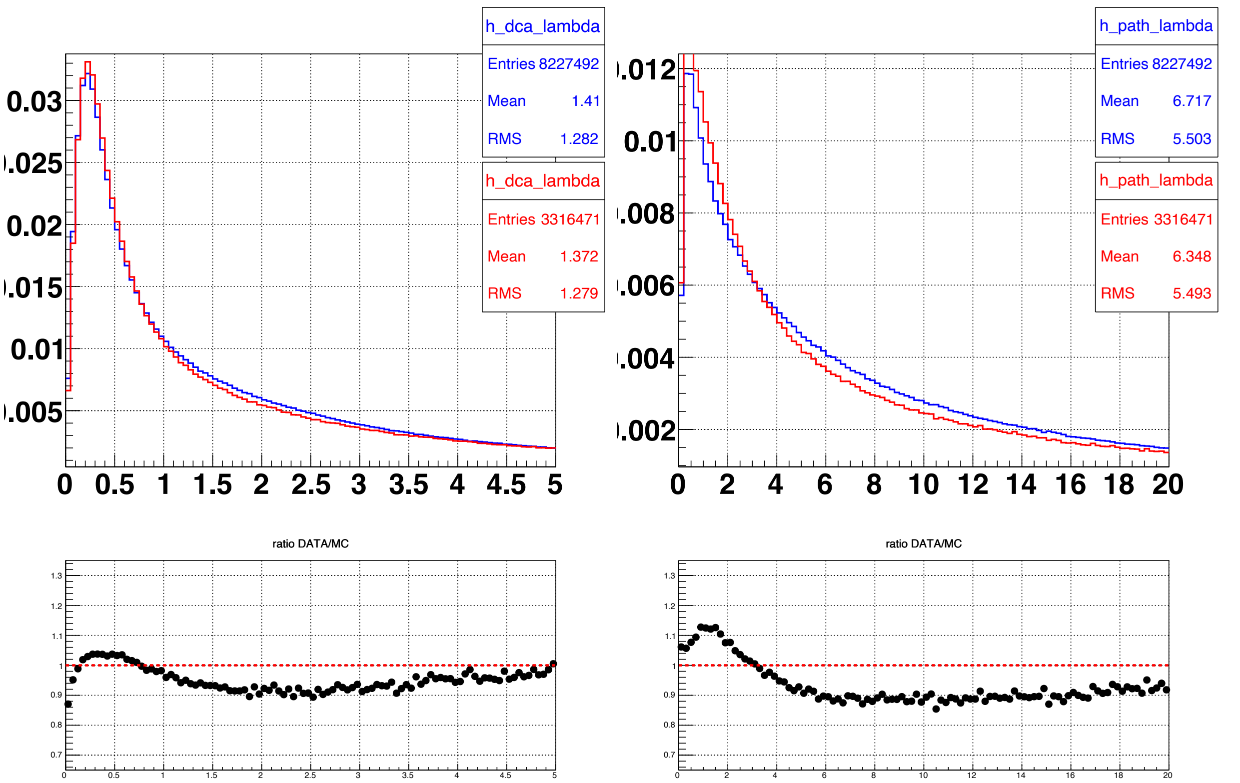

Figure 22. Distance of the closest approach of *V0* decay tracks (*dca*) (left plot) and distance between the primary vertex and *V0* (*path*) (right plot). Ratio of the data/MC presented on bottom pictures. Cuts were applied as follow: *dca<1.0, path>2.5*. Reaction *C+Cu*, energy 4.5 GeV. (redraw with x axis)

Trigger efficiency

The trigger efficiency ε_{trig} calculated for events with reconstructed Λ hyperons in interactions of carbon beam with different targets is given in Table 3. The trigger efficiency was evaluated by a convolution of the MC simulation of the trigger BD detector response with reconstructed Λ hyperons and the GEANT4 MC simulation of delta electrons produced by the carbon beam in the *C, Al, Cu, Pb* targets which were found to be the dominant source of delta electrons. The dependence of the trigger efficiency on the collision impact parameter is presented in Fig.23 for interactions of the carbon beam with the *C, Al, Cu, Pb* targets.

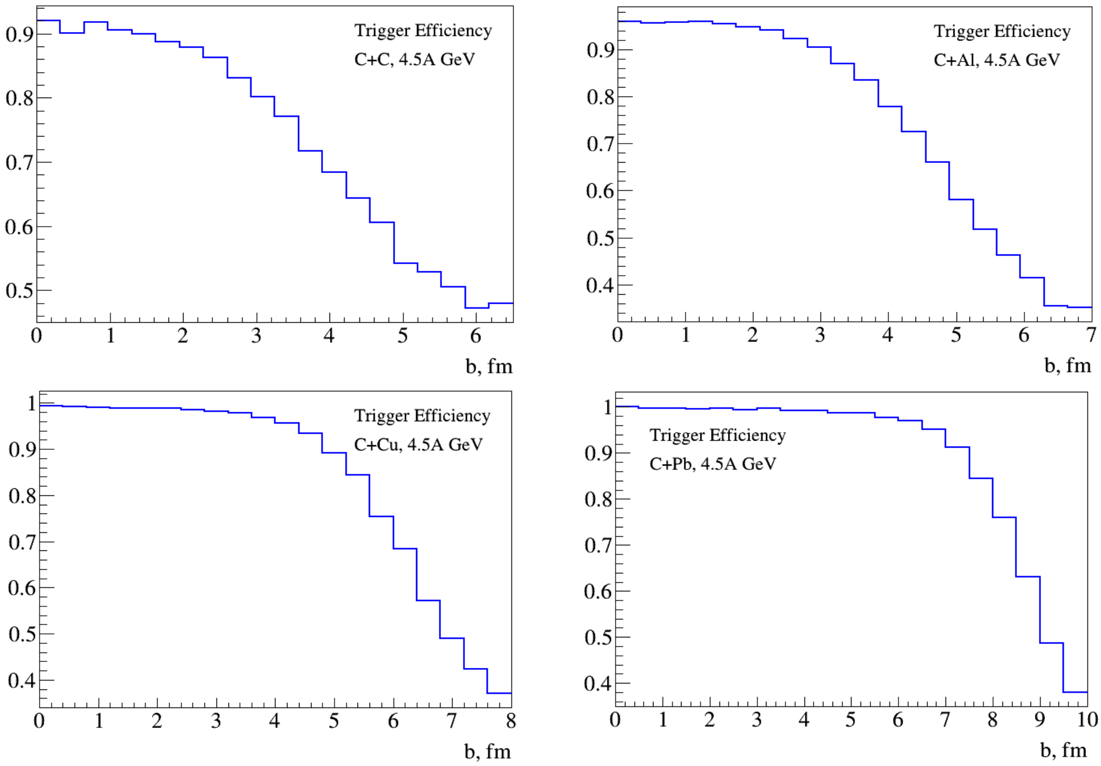

Figure 23. Trigger efficiency (ε_{trig}) as a function of the collision impact parameter. Distributions was obtained for MC events of the carbon beam with the *C, Al, Cu, Pb* targets at 4.5 AGeV.

Table 3. Trigger efficiency estimated with reconstructed Λ hyperons in interactions of the carbon beam with *C, Al, Cu, Pb* targets.

Trigger / Target 4.0 AGeV	*C*	*Al*	*Cu*	*Pb*
ε_{trig} (BD>=2)	0.80±0.02			
ε_{trig} (BD>=3)		0.87±0.02	0.92±0.02	0.95±0.02

Trigger / Target 4.5 AGeV	*C*	*Al*	*Cu*	*Pb*
ε_{trig} (BD>=2)	0.80±0.02			
ε_{trig} (BD>=3)		0.83±0.02	0.91±0.02	0.94±0.02

The systematic errors in Table 3 cover:

1. the contribution of delta electrons background produced in the simulated targets with the fractional thickness from 0.5 to 1 of the real targets;

2. the spread of the trigger efficiency values calculated for different y and p_T bins of reconstructed Λ hyperons;
3. change in the trigger efficiency after adjustment (reweighting) of the simulated track multiplicity to the experimental distributions.

The trigger efficiency obtained in simulation was cross checked by the analysis of data samples with the reduced trigger requirements: BD>=1 for *C+C* interactions and BD>=2 for *C+Al* and *C+Cu* interactions. The evaluated efficiencies for events with reconstructed Λ ε(BD>=2)/ε(BD>=1, *C+C*) = 0.90, ε(BD>=3)/ε(BD>=2, *C+Al*, *C+Cu*, *C+Pb*) = 0.95 are consistent with the same ratios of the trigger efficiencies calculated using simulated events.

Impact parameter distribution

Distributions of the impact parameters of minimum bias interactions generated with the DCM-SMM, UrQMD and PSHD models are shown in Fig. 24. The impact parameter distributions of generated events with Λ hyperons as well as the impact parameters of simulated events with reconstructed Λ hyperons are presented for comparison. The Λ reconstruction requirements and the trigger conditions do not change much the impact parameter distributions. The mean values of the impact parameters for events with Λ hyperons generated in *C+C, C+Al, C+Cu, C+Pb* interactions by the DCM-QGSM model are presented in Table 4.

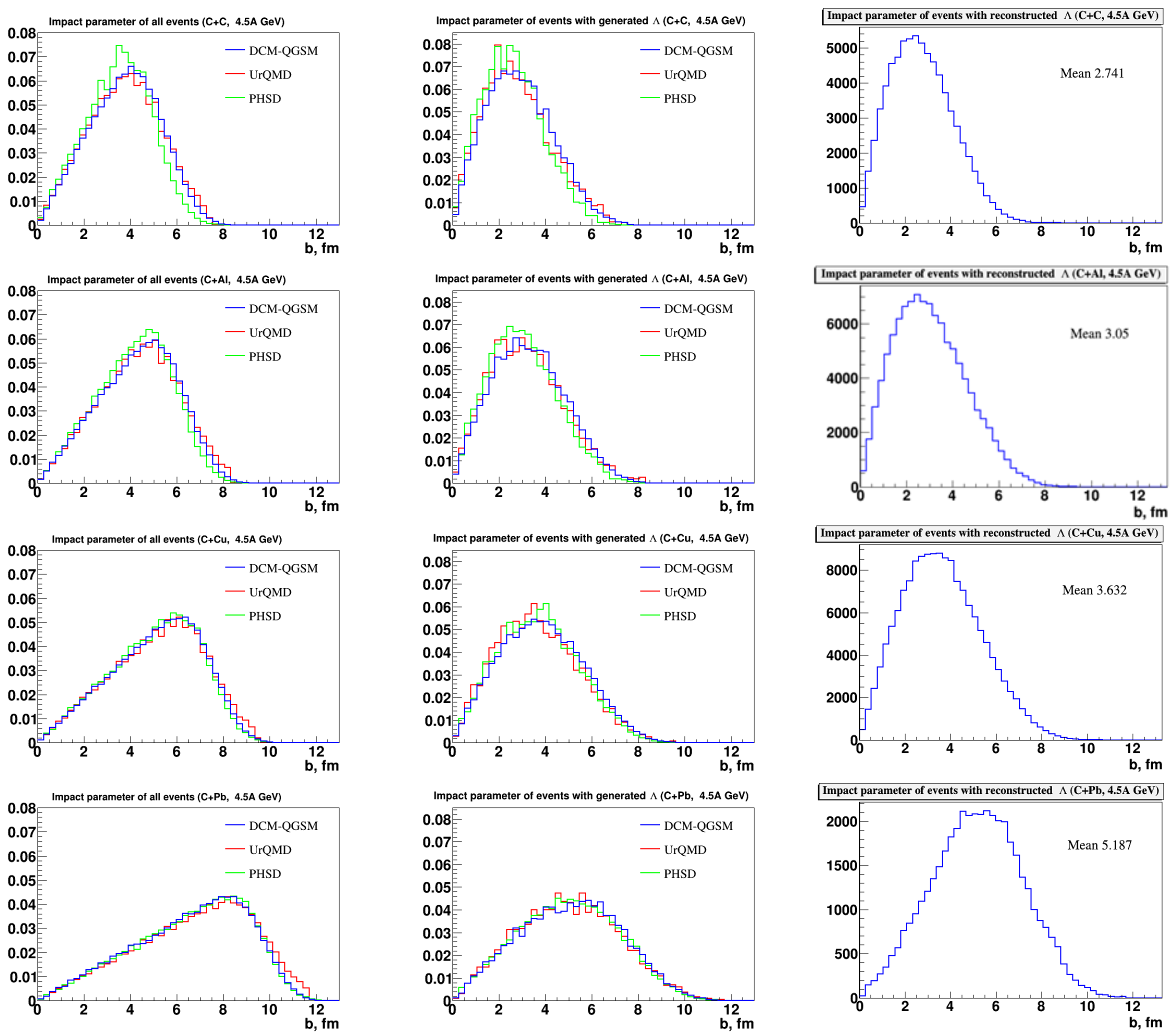

Figure 24. Impact parameter distributions of minimum bias interactions of 4.5 AGeV carbon beam with *C, Al, Cu, Pb* targets for the DCM-QGSM, UrQMD and PHSD models: all generated events (left), generated Λ hyperons (center), reconstructed Λ hyperons (right).

Table 4. Mean impact parameters of min. bias *C+C, C+Al, C+Cu* and *C+Pb* interactions generated by the DCM-QGSM model.

MC	*b*, fm (*C+C*)	*b*, fm (*C+Al*)	*b*, fm (*C+Cu*)	*b*, fm (*C+Pb*)
All min bias events	3.76	4.36	5.13	6.6
Events with Λ	2.80	3.08	3.58	4.8
Events with rec. Λ	2.74	3.05	3.63	5.19

Λ reconstruction efficiency [7]

The Λ reconstruction efficiency was calculated as the ratio of the number of reconstructed Λ hyperons to the number of generated ones in the (y, p_T) intervals, where y is measured in the laboratory frame. The kinematic range [1.2 < y <2.1], [$0.10 < p_T < 1.05\ GeV/c$] was divided into 8×8 cells for simulated (Fig. 25) and reconstructed MC data (Fig. 26). In each *i*-cell, the total number of simulated Λ hyperons was calculated (N_{gen_i}). For the reconstructed MC events the invariant mass distributions were calculated using the pair combinations of the protons and negative pions for each cell. The total number of reconstructed Λ-hyperons was extracted from the obtained invariant mass distributions. The fit function for the background estimation is presented in (1.3). Λ hyperons signal peak region 1.1075-1.125 GeV/c^2 was excluded from the fit procedure.

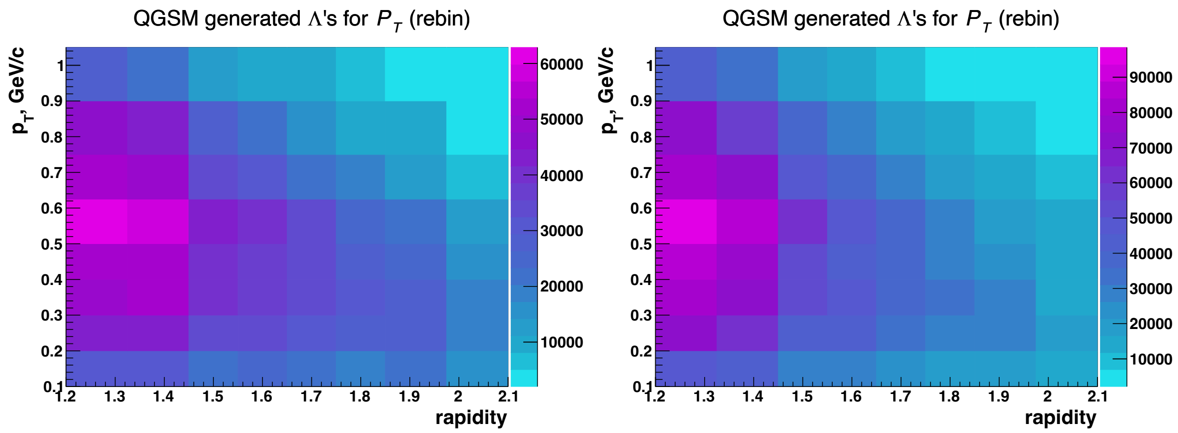

Figure 25. The distribution of the generated of Λ hyperons in (y, pT) bins for 4.0 AGeV energy: $C + C$ interactions (left) and $C + Cu$ interactions (left).

Number of the reconstructed Λ hyperons N_{rec_i} (signal) was calculated as difference between all events in the signal peak region and events obtained under fit function shape (background) (Fig. 27). The background was determined in the 1.1075-1.125 GeV/c^2 mass range window.

$$f_{bg} = N \cdot (m - M_0)^A \cdot e^{-B\cdot(m-M_0)} \tag{1.3}$$

where N, A , B – free parameters of the fit function;
$M_0 = 1.078\ GeV/c^2$ – invariant mass of the Λ;
m – mass of the (p, π^-) reconstructed pair.

The ratio of the reconstructed Λ-hyperons to the total number of generated Λ-hyperons gives the reconstruction efficiency:

$$\omega_{acc} = N_{rec\_i}/N_{gen\_i} \tag{1.4}$$

The possible variation of the reconstruction efficiency was calculated using the bootstrapping method applied to the reconstructed mass distributions in the (y, p_T) cells. Each bin value of the invariant mass spectra was 1000 times randomly resampled according to the Gaussian function, where the mean parameter corresponded to the bin value and sigma parameter corresponded to it error. The new variated histograms were fitted by the Gaussian function and the errors due to the statistical fluctuations of the signal were obtained from the fits. The histograms in Fig. 28 show the distributions of the signal variation for different (y, p_T) bins for the reconstructed MC events.

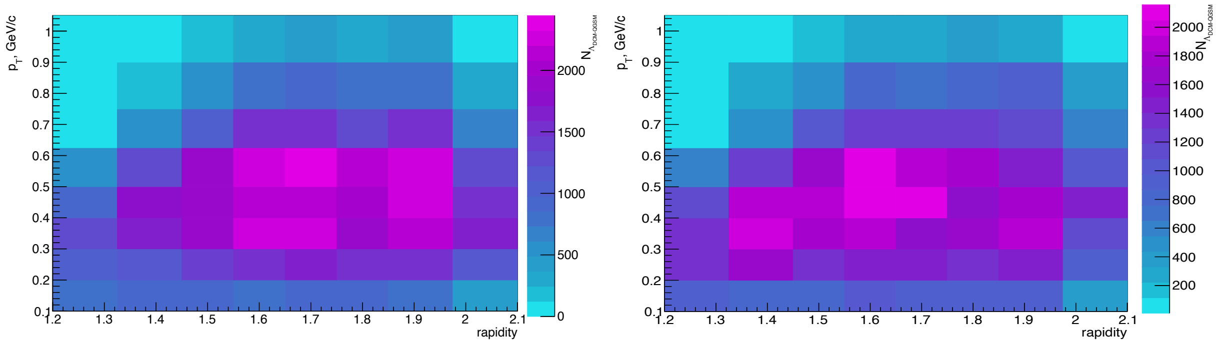

Figure 26. The MC distribution of the reconstructed signals with beam energy 4.5AGeV for $C + C$ (left) and $C + Cu$ (right) reactions.

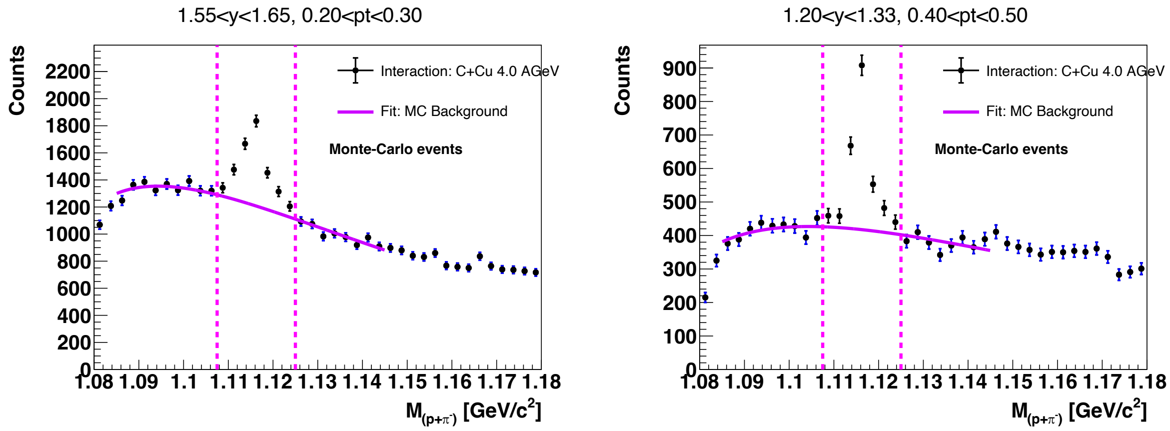

Figure 27. The mass distribution and background fit in the different (y, p_T) cells for 4.5AGeV C+Cu. The magenta line is the background fit function (1.3).

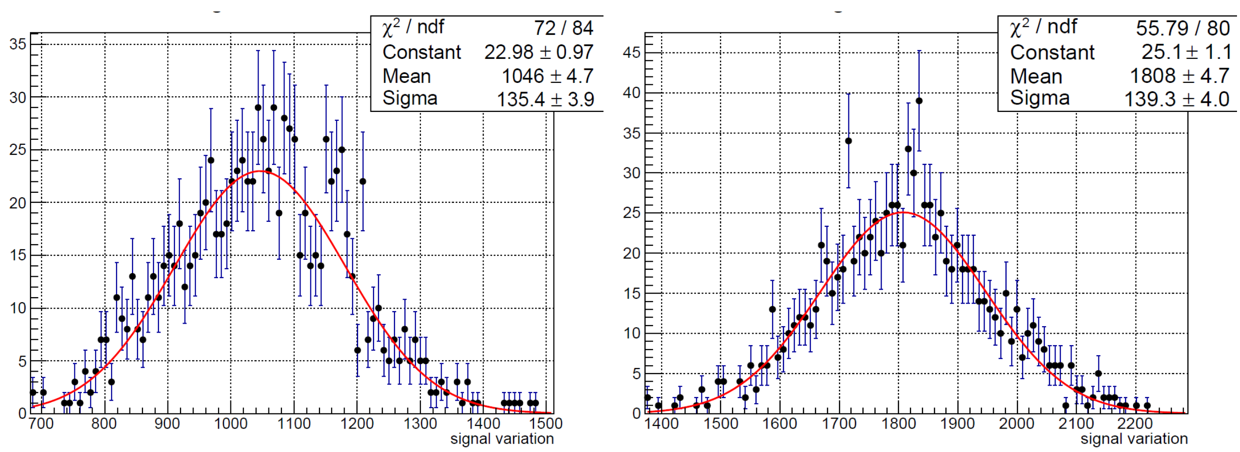

Figure 28. $C + Cu$ reaction. MC distribution of signal variation for two kinematic cells: 1.2< y <1.33, 0.1<p_T< 0.2 (left), 1.33< y <1.45, 0.2<p_T< 0.3 (right)

The uncertainty of the reconstruction efficiency determination was calculated as:

$$\Delta\omega_{acc} = \sigma_{N_{rec\_i}{}_{MC}} / N_{gen\_i} \qquad (1.5)$$

where N_{gen_i} - the total number of generated Λ-hyperons in corresponded i-cell.

The distributions of the Λ hyperon signal reconstruction efficiency in the *(y, p_T)* kinematic regions are shown in Fig. 28 and Fig. 29 for 4.0 GeV and 4.5 AGeV energy respectively. Kinematic cells with efficiency $\omega_{acc} < 0.01$ were excluded from the analysis, they are shown in white in the pictures.

For the reconstruction efficiency correction in cells with $\omega_{acc} < 0.01$ the extrapolation factor values f_{extrap} were calculated using DCM-QGSM model. They are were calculated as a ratio of the number of all MC generated Λ hyperons in cell column along p_T to the number of MC reconstructed Λ hyperons with the reconstruction efficiency above $\omega_{acc} > 0.01$ in this column. The extrapolation factor is determined using the formula:

$$f_{extrap} = {N_{all\_gen}}/{N_{all\_rec}} \qquad (1.6)$$

where: N_{all_gen} - is the sum of all generated events in cell column along p_T;

N_{all_rec} - is the sum of reconstructed events with $\omega_{acc} \geq 0.01$ in the considered cell column along p_T;

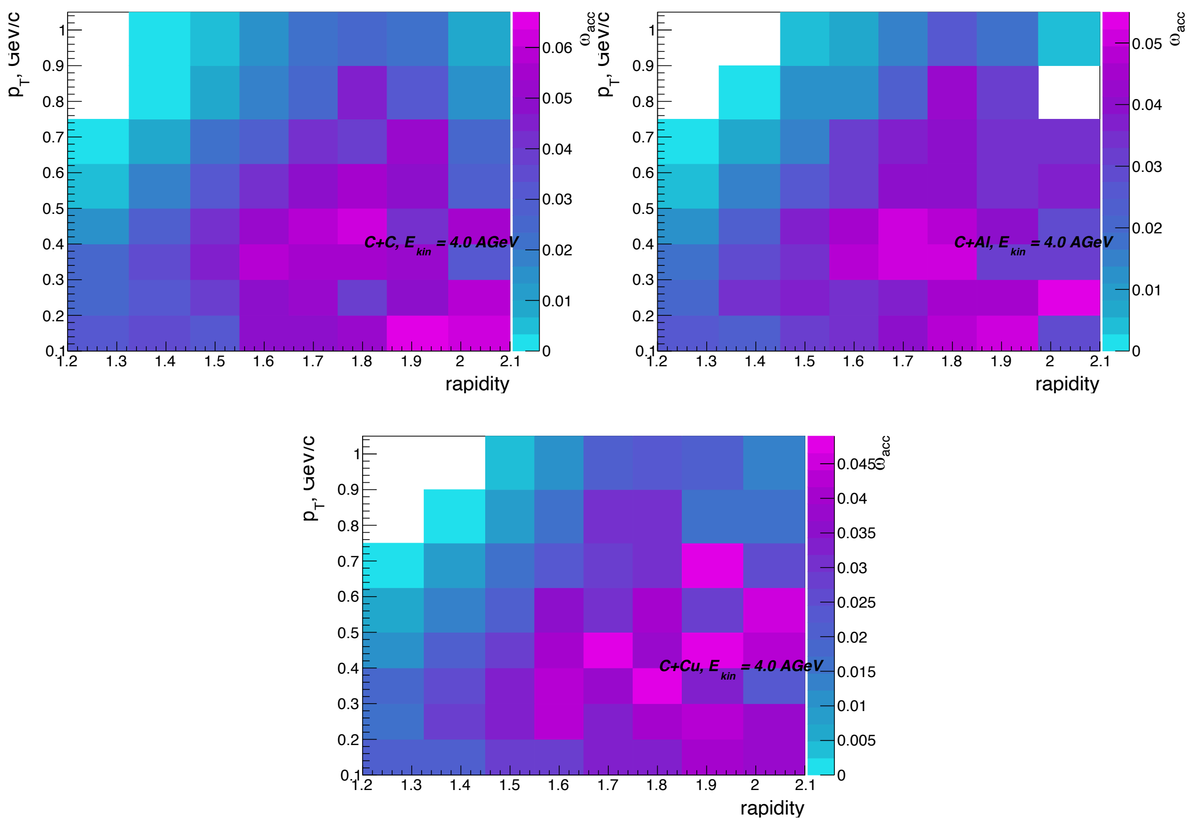

Figure 28. The MC distribution of Λ reconstruction efficiency in (*y,pT*) bins for 4.0 AGeV energy: *C+C* interactions (top left); *C+Al* interactions(top right); *C+Cu* interactions (bottom left). Due the low statistics in the physical data the *C+Pb* process at 4.0AGeV was excluded from the analysis.

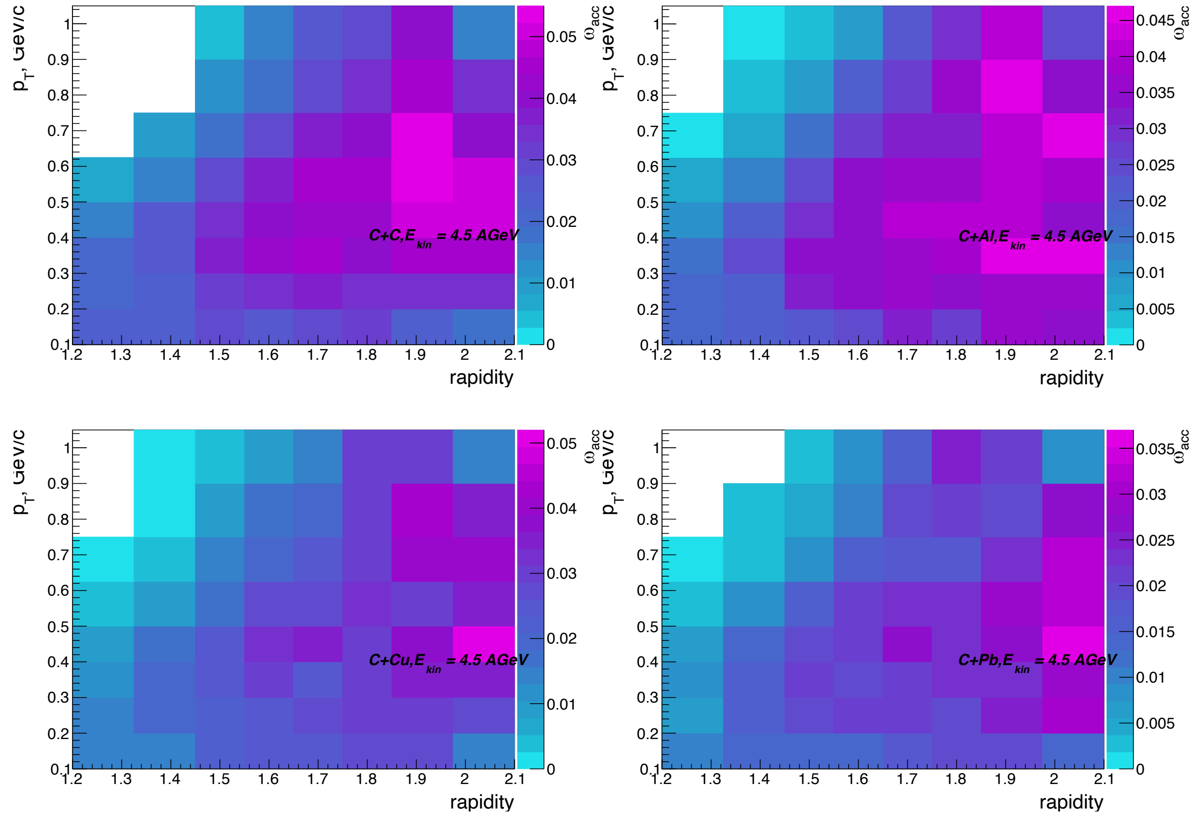

Figure 29. The MC distribution of *Λ* reconstruction efficiency in (*y,pT*) bins for 4.5 AGeV energy: *C+C* interactions (top left); *C+Al* interactions(top right); *C+Cu* interactions (bottom left), *C+Pb* interactions (bottom right).

Due to the low statistics in the physical data for the *Λ* cross sections and yield values calculations the obtained MC extrapolation factors were summed into 4×4 cells matrix in the (*y*, p_T) kinematic range. The extrapolation factor for the efficiency corrections for cells with $\omega_{acc} < 0.01$ was determined for each *C+A* reaction separately. They are presented in Table 5.

Table 5. The values of the MC generated *Λ*-hyperons, number of the reconstructed MC *Λ*-hyperons and calculated extrapolation factors.

***y* range**	**Tkin = 4.0 AGeV**		
	C+C		
1.20 - 1.45	712131	409932	2.03 ± 0.003
1.45 - 1.65	497063	455375	1.09 ± 0.002
1.85 - 2.10	245509	243472	1.01 ± 0.003
	C+Al		
1.20 - 1.45	930423	538999	1.73 ± 0.003
1.45 - 1.65	594258	562752	1.06 ± 0.002
1.85 - 2.10	257086	255172	1.01 ± 0.003
	C+Cu		
1.20 - 1.45	1088598	730706	1.48 ± 0.002
1.45 - 1.65	634805	531683	1.19 ± 0.002
1.85 - 2.10	239136	229466	1.00 ± 0.003

***y* range**	**Tkin = 4.5 AGeV**		
	C+C		
1.20 - 1.45	956603	441817	2.17±0.004
1.45 - 1.65	723551	695781	1.04±0.002

1.85 - 2.10	452888	447921	1.00±0.002
	C+Al		
1.20 - 1.45	1271777	611399	2.08 ± 0.003
1.45 - 1.65	881912	764628	1.15 ± 0.002
	C+Cu		
1.20 - 1.45	1538870	739101	2.08 ± 0.003
1.45 - 1.65	967469	840427	1.15 ± 0.002
	C+Pb		
1.20 - 1.45	770025	366149	2.10±0.004
1.45 - 1.65	485904	384981	1.26±0.003
1.85 - 2.10	238339	235515	1.01±0.002

Λ hyperon signal in data

The signal from *Λ* hyperon decays is observed as a narrow peak in the invariant mass distribution of the two tracks with opposite charge with the proton and pion mass hypothesis. For each event in the experimental data set, the weight ω_{acc} equal to the reconstruction efficiency (see 1.4) in the (y, p_T) bin was assigned, according to corresponding kinematic cell this event belongs. The invariant mass distributions were calculated for each cell with a $1.0/\omega_{acc}$ weight. After the cell contents were summed separately by column $\sum_{ij} pT_{ij}$ and by row $\sum_{ij} y_{ij}$, respectively. Mass distribution was obtained in kinematic range $0.10 < p_T < 1.05\ GeV/$c, 1.2 < y <2.1 as for the MC.

For the background estimation, the mass distributions were fitted using a combination of the threshold and exponential functions (see 1.3). The fits ranges were chosen according to the best ratio of the $\chi^2/ndf\sim1$. The mass window for *Λ* signal extraction was set within 1.1075-1.125 GeV/c^2 range and was excluded from the fit. The numbers of *Λ* hyperons were determined from the content of the background-subtracted histogram bins within mass window.

Spectra of the invariant mass of (p, π^-) for weighted experimental data events reconstructed in interactions of 4.0AGeV and 4.5AGeV carbon beam with the background fit function for the different targets are shown in Fig. 30 and 31, respectively. The statistics of *Λ* hyperons reconstructed in *C+C, C+Al, C+Cu, C+Pb* interactions in bins of y and p_T are summarized in Tables 6 and 7 for 4.0 AGeV and 4.5 AGeV carbon beam data, respectively.

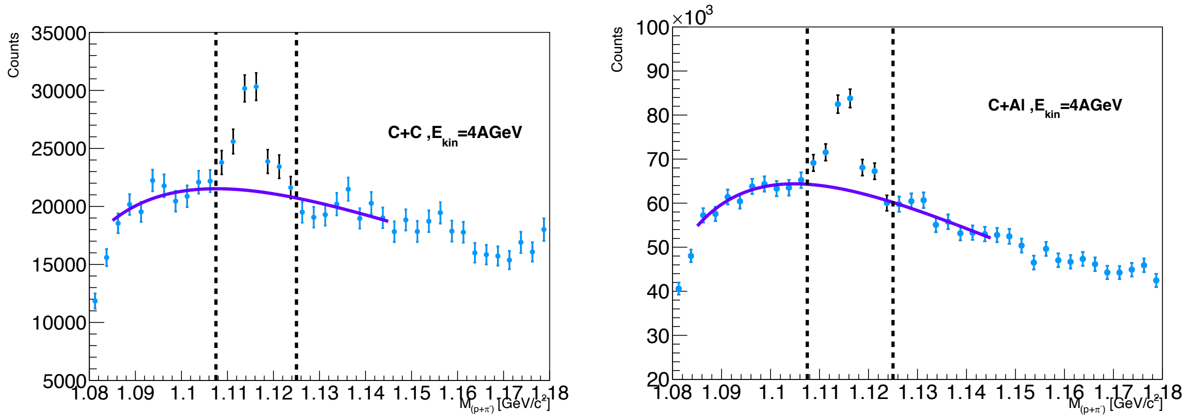

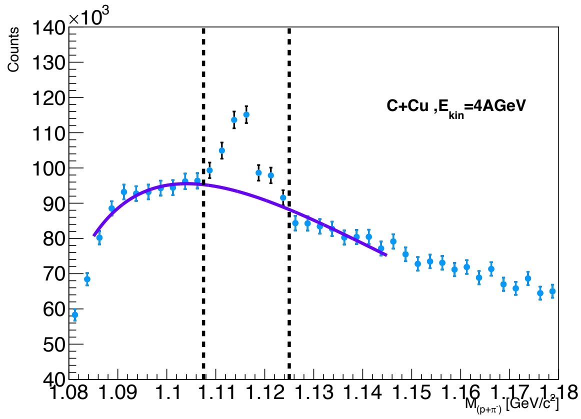

Figure 30. $\Lambda \rightarrow p\pi^-$ signal reconstructed in *C+C* (top left*), C+Al* (top right)*, C+Cu*(bottom) interactions at 4.0 AGeV carbon beam energy. The violet line is background fit function. The Λ signal mass window indicated by the vertical lines. Due the low statistics in the physical data the *C+Pb* process at 4.0AGeV was excluded from the analysis.

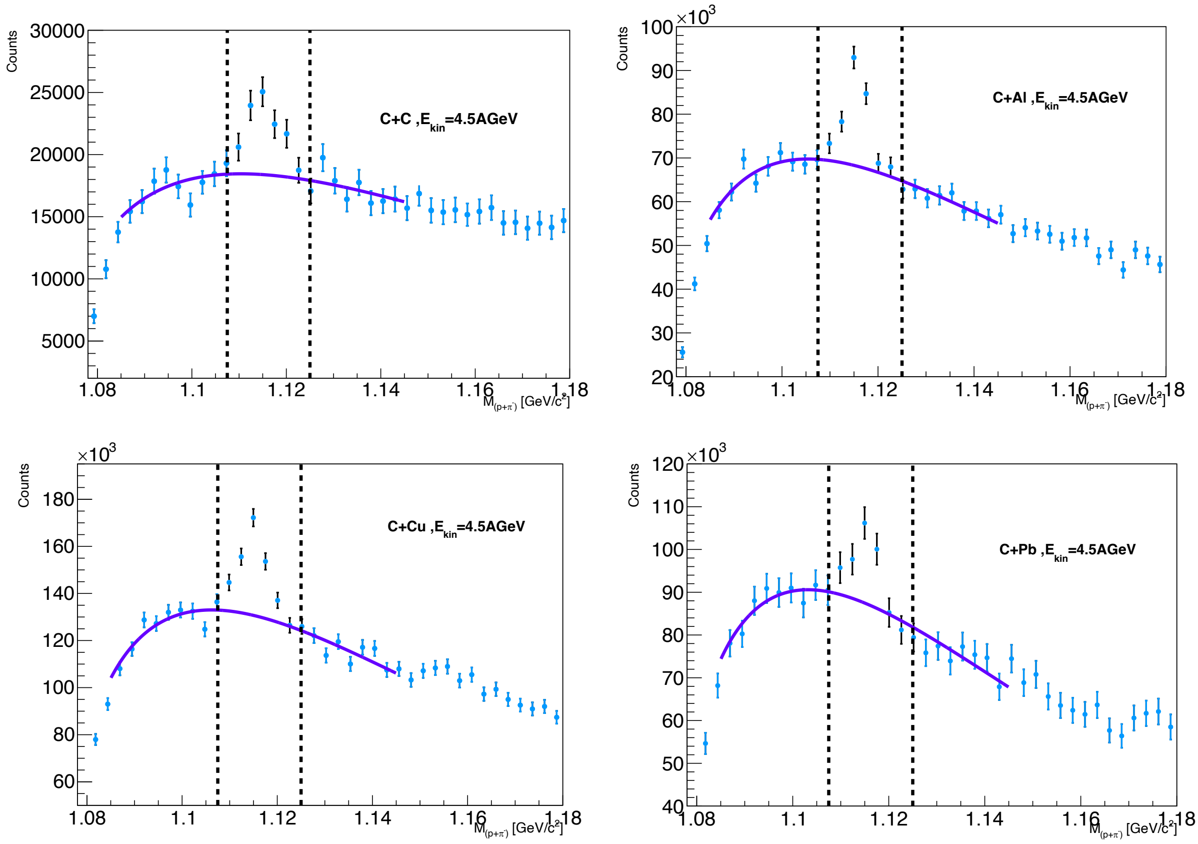

Figure 31. $\Lambda \rightarrow p\pi^-$ signal reconstructed in *C+C* (top left*), C+Al* (top right)*, C+Cu* (bottom left)*, C+Pb* (bottom right)*,* interactions at 4.5 AGeV carbon beam energy. The violet line is background fit function. The Λ signal mass window indicated by the vertical lines.

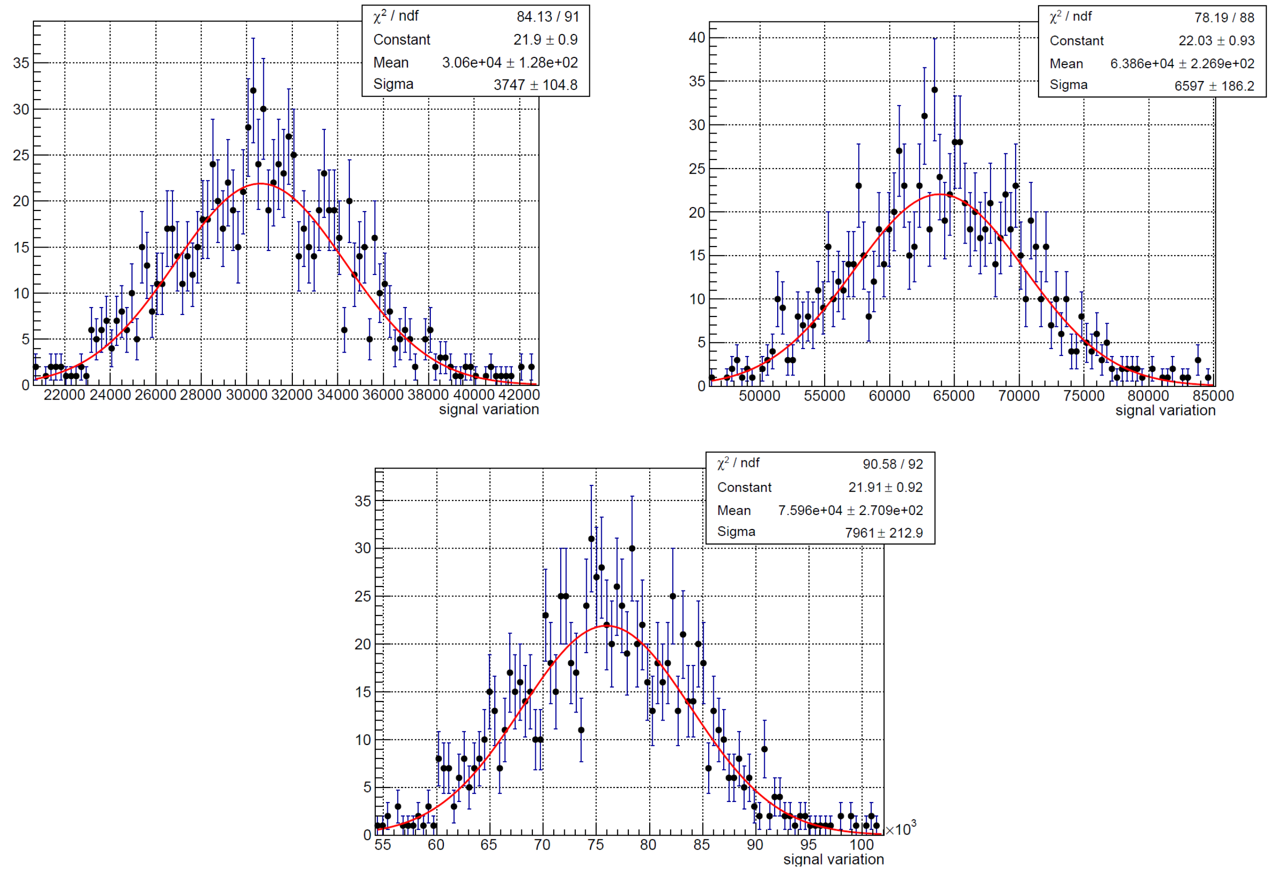

Figure 32. Distributions of signal variation for the data in the kinematic range 0.1 $<p_T<$1.05 and 1.2 $<y<$2.1 for interactions at 4.0 AGeV beam energy: *C+C* (top left), *C+Al* (top right), *C+Cu* (bottom).

The uncertainties of the reconstructed Λ hyperons signal due data fluctuations were calculated using the same procedure as for MC. The distributions of the signal variation for *C+C*, *C+Al*, *C+Cu* and *C+Pb* interactions at beam energies of 4.0 AGeV and 4.5 AGeV are shown in Figures 32 and 33.

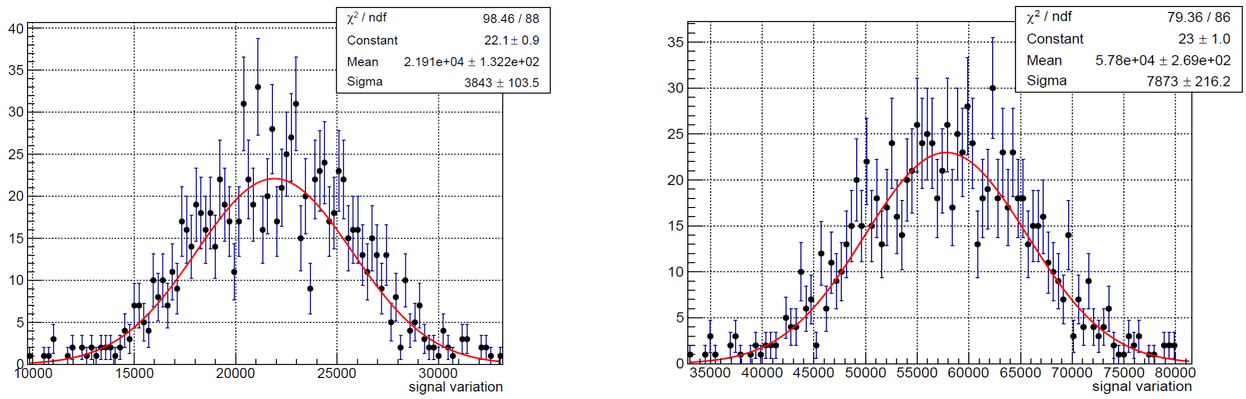

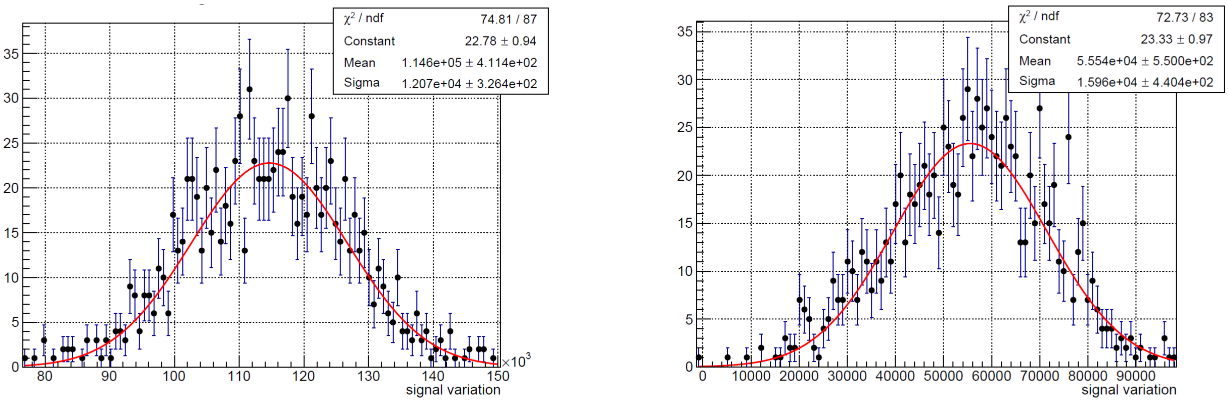

Figure 33. Distribution of signal variation for the data in the kinematic range 0.1 $<p_T<$1.05 and 1.2 $<y<$2.1 for interactions at a beam energy of 4.5 AGeV: *C+C* (top left*), C+Al* (top right)*, C+Cu* (bottom)*, C+Pb* (bottom right)

Table 6. Reconstructed weighted signals of Λ hyperons in bins of y and p_T in 4.0 AGeV carbon-target interactions. The first error presents the statistical uncertainty, the second error is systematic.

Target / y interval	C	Al	Cu	Pb
1.2-1.45	11614 ± 2524 ± 222	30925 ± 4704 ± 594	26692 ± 5670 ± 512	Low statistic
1.45-1.65	5832 ± 1261 ± 112	17766 ± 2516 ± 340	23881 ± 3538 ± 650	
1.65-1.85	5517 ± 1090 ± 106	7211 ± 1846 ± 138	16720 ± 2728 ± 619	
1.85-2.1	3803 ± 1351 ± 73	3437 ± 2277 ± 66	15700 ± 3419 ± 563	

Target / p_T interval	C	Al	Cu	Pb
0.1-0.3	7937 ± 2037 ± 152	15099 ± 3594 ±290	24242 ± 5046 ± 535	Low satatistic
0.3-0.5	9312 ± 2050 ± 179	24374 ± 3924 ± 468	27560 ± 4921 ± 533	
0.5-0.85	8189 ± 1336 ± 157	14617 ± 2276 ± 281	20399 ± 2983 ± 562	
0.85-1.05	1148 ± 854 ± 22	5100 ± 1587 ± 98	10269 ± 2295 ± 368	

Table 7. Reconstructed weighted signals of Λ hyperons in bins of y and p_T in 4.5 AGeV carbon-target interactions. The first error presents the statistical uncertainty, the second error is systematic.

Target / y interval	C	Al	Cu	Pb
1.2-1.45	10049 ± 2994 ±193	24280 ± 6609±466	45119 ± 10437 ± 866	21456 ± 8001 ± 411
1.45-1.65	4390 ± 1199 ± 84	20443 ± 2840±392	31769 ± 4261± 610	13222 ± 4052 ± 254
1.65-1.85	2648 ± 1222± 51	9706 ± 2406±186	23971 ± 3719 ± 460	11175 ± 2984 ± 214
1.85-2.1	6565 ± 1516 ±126	8896 ± 2407±171	24144 ± 3885 ±463	4891 ± 2952 ± 94

Target / p_T interval	C	Al	Cu	Pb
0.1-0.3	4353 ± 2756±84	17244 ± 5563±331	39227 ± 8591 ± 753	11267 ± 6771 ± 216
0.3-0.5	11470 ± 2138±220	28201 ± 4919±541	44722 ± 6808 ± 858	21450 ± 7620 ± 412
0.5-0.85	4851 ± 1384±93	13458 ± 2406±258	31402 ± 4994 ±603	14307 ± 2811 ± 275
0.85-1.05	2924 ± 724±56	4462 ± 1296±86	9810 ± 2101 ± 188	3439 ± 1790 ± 66

Evaluation of Λ hyperon cross sections and spectra:

The inclusive cross section σ_Λ and yield Y_Λ of Λ hyperon production in $C+C$, $C+Al$, $C+Cu$, $C+Pb$ interactions are calculated in bins of y (p_T) according to the next formulas:

$$\sigma_\Lambda(y) = \sum_{p_T}(N_{rec}^{\Lambda}(y,p_T)/\varepsilon_{rec}(y,p_T))/(\varepsilon_{trig} \times \varepsilon_{pileup} \times L) \quad (1.7)$$

$$\sigma_\Lambda(p_T) = \sum_{y}(N_{rec}^{\Lambda}(y,p_T)/\varepsilon_{rec}(y,p_T))/(\varepsilon_{trig} \times \varepsilon_{pileup} \times L) \quad (1.8)$$

$$Y_\Lambda(y) = \sigma_\Lambda(y)/\sigma_{inel} \quad (1.9)$$

$$Y_\Lambda(p_T) = \sigma_\Lambda(p_T)/\sigma_{inel} \quad (1.10)$$

where: L is the luminosity (Table 2);

$N_{rec}^{\Lambda}/\ \varepsilon_{rec}$ - the number of reconstructed Λ hyperons, corrected to ε_{rec} – the combined efficiency of the Λ hyperon reconstruction (Tables 6 and 7);

ε_{trig} – the trigger efficiency (Table 3);

ε_{pileup} – the beam halo and pile-up suppression factor (Table 1),

σ_{inel}–the cross section for minimum bias inelastic $C+A$ interactions (Table 8).

The cross section for inelastic C+C interactions is taken from the measurement [8]. The cross sections for inelastic $C+Al$, $C+Cu$, $C+Pb$ interactions are taken from the predictions of the DCM-QGSM model which are consistent with the results calculated by the formula:

$$\sigma_{inel} = \pi R_0^2 (A_P^{\frac{1}{3}} + A_T^{\frac{1}{3}})^2 \quad (1.11)$$

where: R_0 = 1.2 fm is an effective nucleon radius,

A_P and A_T are atomic weight of the beam and target nucleus [9].

The uncertainties for $C+Al$, $C+Cu$, $C+Pb$ inelastic cross sections are estimated by using the alternative formula:

$$\sigma_{inel} = \pi R_0^2 (A_P^{\frac{1}{3}} + A_T^{\frac{1}{3}} - b)^2 \quad (1.12)$$

with R_0 = 1.46 fm and b = 1.21 [8].

Table 8. Inelastic cross sections for carbon-nucleus interactions.

Interaction	***C+C***	***C+Al***	***C+Cu***	***C+Pb***
Inelastic cross section, mb	830±50	1260±50	1790±50	3075±50

The yields of Λ hyperons in minimum bias $C+C$, $C+Al$, $C+Cu$, $C+Pb$ interactions are measured in the kinematic range on the Λ transverse momentum of $0.1<p_T<1.05$ GeV/c and the Λ rapidity in the laboratory frame of $1.2<y<2.1$.

The rapidity of the beam-target nucleon-nucleon in center of mass (CM) system was calculated. The transformation of the y distribution to c.m.s. gives $y^*=y-y_{CM}$. The corrected differential y^* spectra of Λ hyperon yields are presented in Figs. 34 and 35 for 4.0 AGeV and 4.5 AGeV carbon beam energies, respectively. The differential p_T spectra of Λ hyperon yields are presented in Figs. 36 and 37. The predictions of the DCM-SMM, URQMD and PHSD models were calculated and shown for comparison. Due the low statistics in the physical data the $C+Pb$ process at 4.0AGeV was excluded from the analysis.

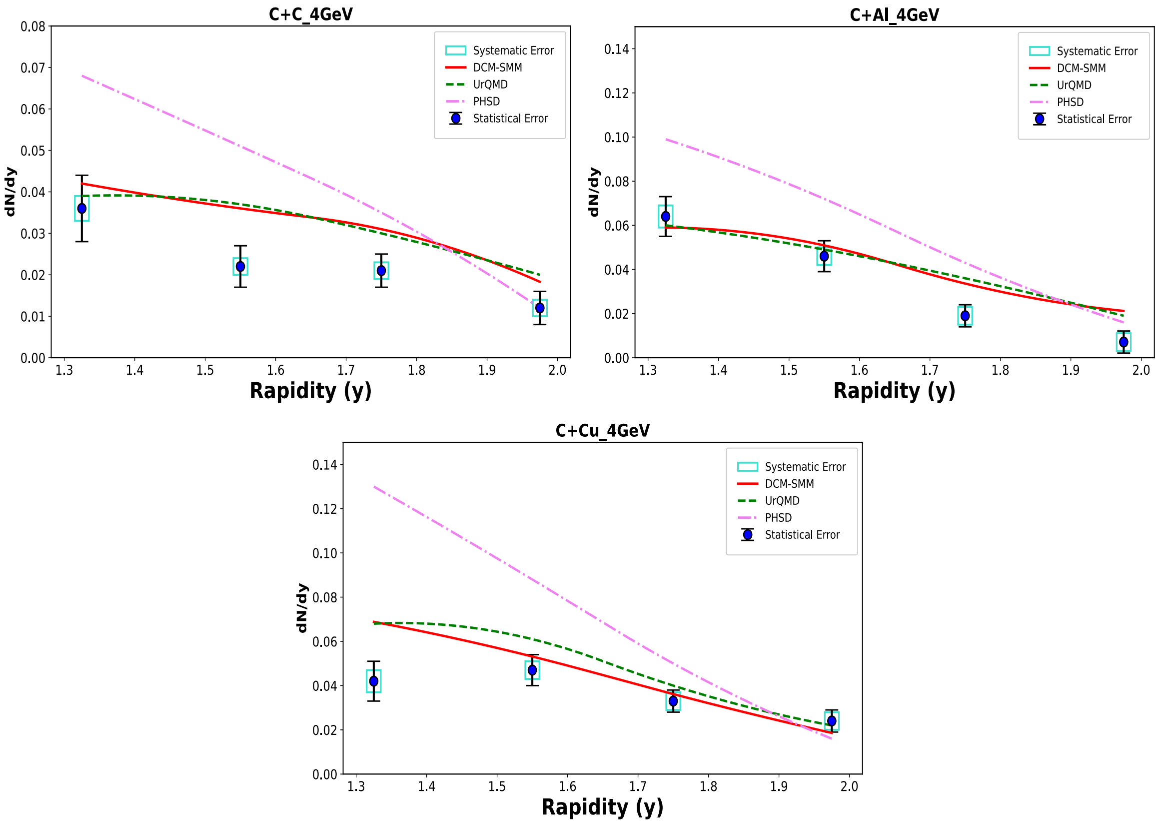

Figure 34. Reconstructed rapidity *y* spectra of *Λ* hyperons in minimum bias *C+C, C+Al, C+Cu* interactions at 4.0 AGeV carbon beam energy. The error bars represent the statistical errors, the blue boxes show the systematic errors. Predictions of the DCM-SMM, UrQMD and PHSD models are shown as colored lines.

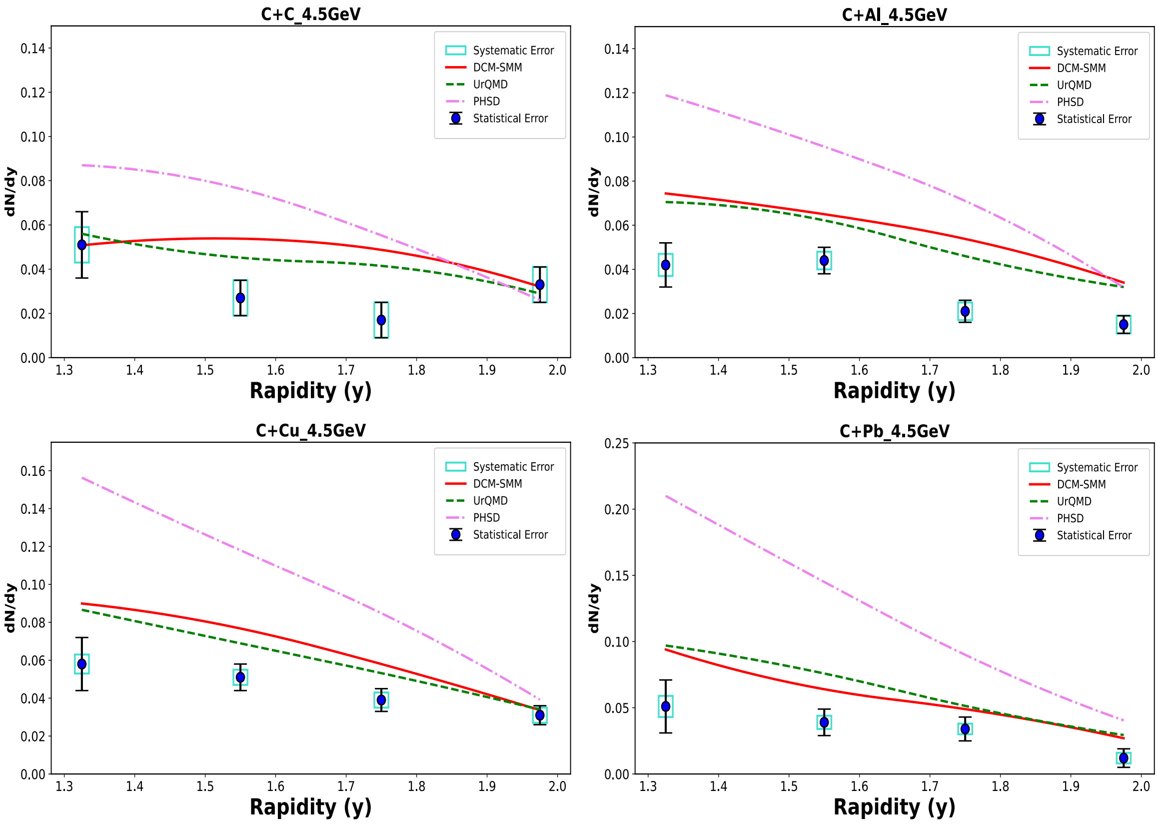

Figure 35. Reconstructed rapidity *y* spectra of *Λ* hyperons in minimum bias *C+C, C+Al, C+Cu, C+Pb* interactions at 4.5 AGeV carbon beam energy. The error bars represent the statistical errors, the blue

boxes show the systematic errors. Predictions of the DCM-SMM, UrQMD and PHSD models are shown as colored lines.

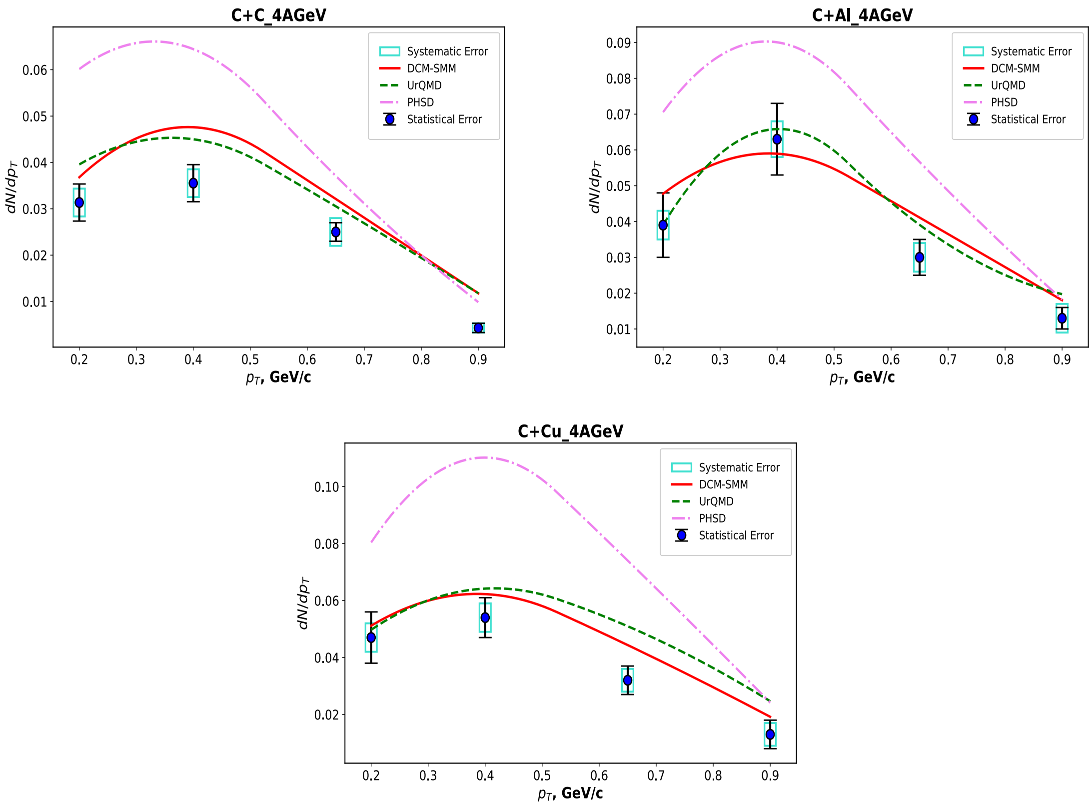

Figure 36. Reconstructed transverse momentum p_T spectra of Λ hyperons in minimum bias *C+C, C+Al, C+Cu* interactions at 4.0 AGeV carbon beam energy. The error bars represent the statistical errors, the blue boxes show the systematic errors. Predictions of the DCM-SMM, UrQMD and PHSD models are shown as colored lines.

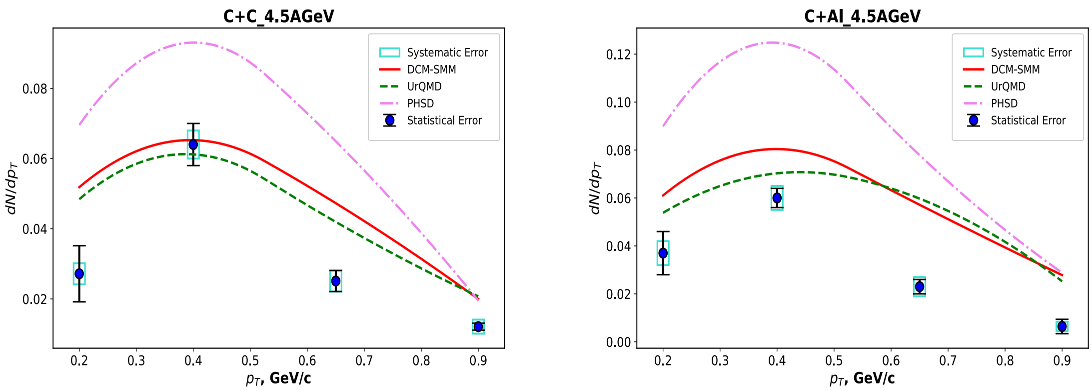

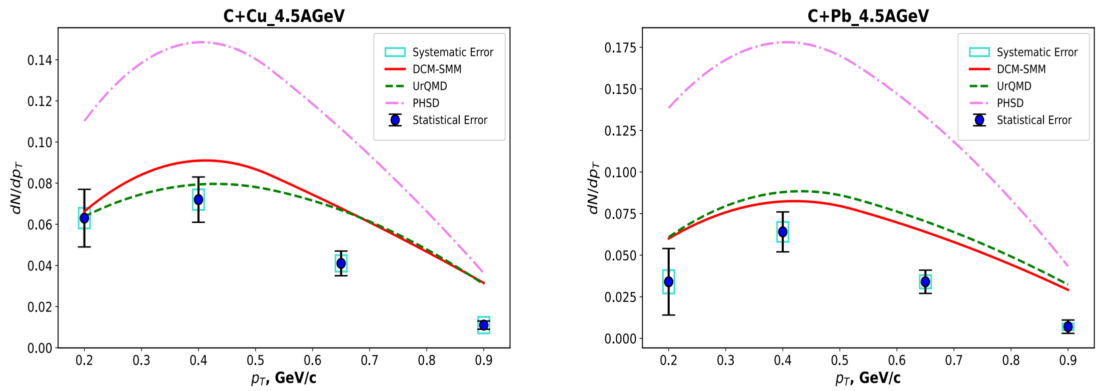

Figure 37. Reconstructed transverse momentum p_T spectra of Λ hyperons in minimum bias *C+C, C+Al, C+Cu, C+Pb* interactions at 4.5 AGeV carbon beam energy. The error bars represent the statistical errors, the blue boxes show the systematic errors. Predictions of the DCM-SMM, UrQMD and PHSD models are shown as colored lines.

The measured differential spectra of the Λ yields in p_T region were parameterized by the form:

$$\frac{1}{p_T}\frac{d^2N}{dp_T dy} = N \times \exp\left(-\frac{m_T - m_\Lambda}{T_0}\right) \quad (1.13)$$

where: $m_T = \sqrt{m_\Lambda^2 + p_T^2}$ - transverse mass;
N – normalization parameter;
T_0 – inverse slope parameter;
dy - corresponds to the measured y range.

T_0 parameter was estimated for the experimental Λ spectra and was compared with the predictions of the DCM-SMM, URQMD and PHSD models Fig. 38 and Fig. 39 for the 4.0 AGeV and 4.5AGeV respectively. Due the low statistics and unstable fit the *C+Pb* process was excluded from the T_0 calculations for 4.0 AGeV energy. The values of the inverse slope T_0, extracted from the fit of the p_T spectra are summarized in Table 9.

The systematic errors of the slope parameters values were estimated using series of the analysis with different cut values for the Λ-hyperon events selection. For the each set of cut values the transverse momentum p_T spectra was fitted according function (1.13) and T_0 parameter was extracted from the fit. The differencies between the obtained slope parameter values with different selection criteria were used to estimate the systematic error.

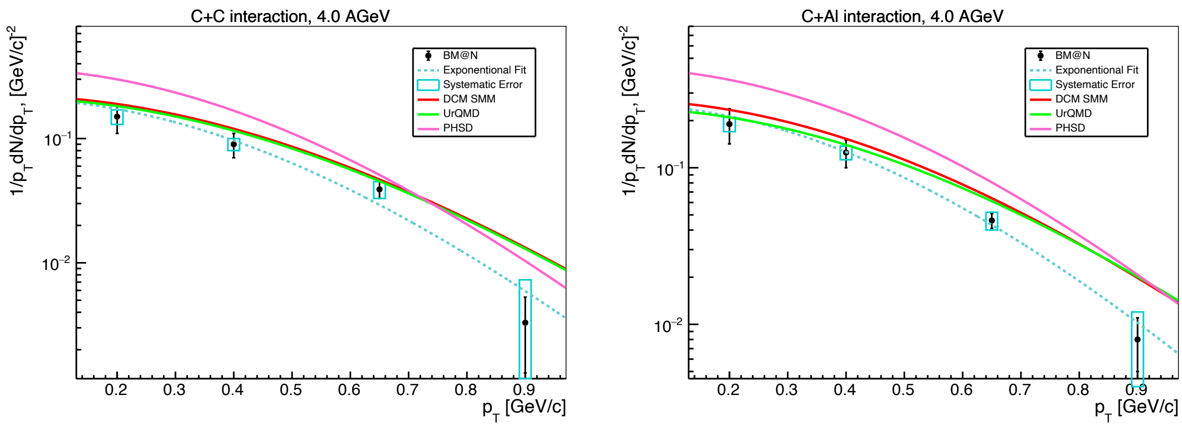

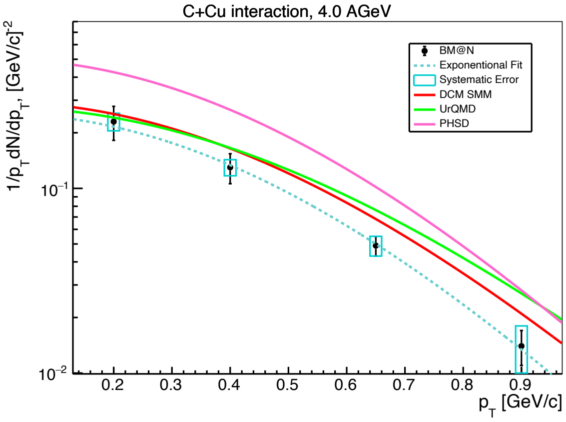

Figure 38. Invariant transverse momentum p_T spectra of Λ hyperons in minimum bias *C+C* (top left*)*, *C+Al* (top right)*, C+Cu* (bottom) interactions at 4.0 AGeV carbon beam energ. The error bars represent the statistical errors, the blue boxes show the systematic errors. The blue lines represent the results of the parameterization described in the text. The predictions of the DCM-SMM, UrQMD and PHSD models are shown as colored lines.

Table 9. Inverse slope parameter T_0 extracted from the fit of the invariant p_T spectra.

4.0 AGeV	***T₀*, MeV (*C+C*)**	***T₀*, MeV (*C+Al*)**	***T₀*, MeV (*C+Cu*)**	***T₀*, MeV *(C+Pb)***
BM@N	89 ±9± 17	99 ± 10 ±16	108 ± 11 ± 14	Low statistic
χ2/ndf	1.83	0.57	0.1	
DCM-SMM	109 ± 1	117± 3	117± 3	123± 4
UrQMD	114 ± 7	128 ± 7	137± 6	135± 8
PHSD	89 ± 3	105 ± 3	111 ± 7	102 ± 4

4.5 AGeV	***T₀*, MeV (*C+C*)**	***T₀*, MeV (*C+Al*)**	***T₀*, MeV (*C+Cu*)**	***T₀*, MeV *(C+Pb)***
BM@N	107 ± 17 ± 17	86 ± 8 ±17	91 ± 8 ±15	99 ± 17 ± 20
χ2/ndf	1.00	0.77	0.19	0.78
DCM-SMM	118 ± 2	126 ± 4	129 ± 6	130 ± 5
UrQMD	125 ± 4	132 ± 7	138 ± 8	143 ± 6
PHSD	109 ± 5	113 ± 5	115 ± 5	113 ± 5

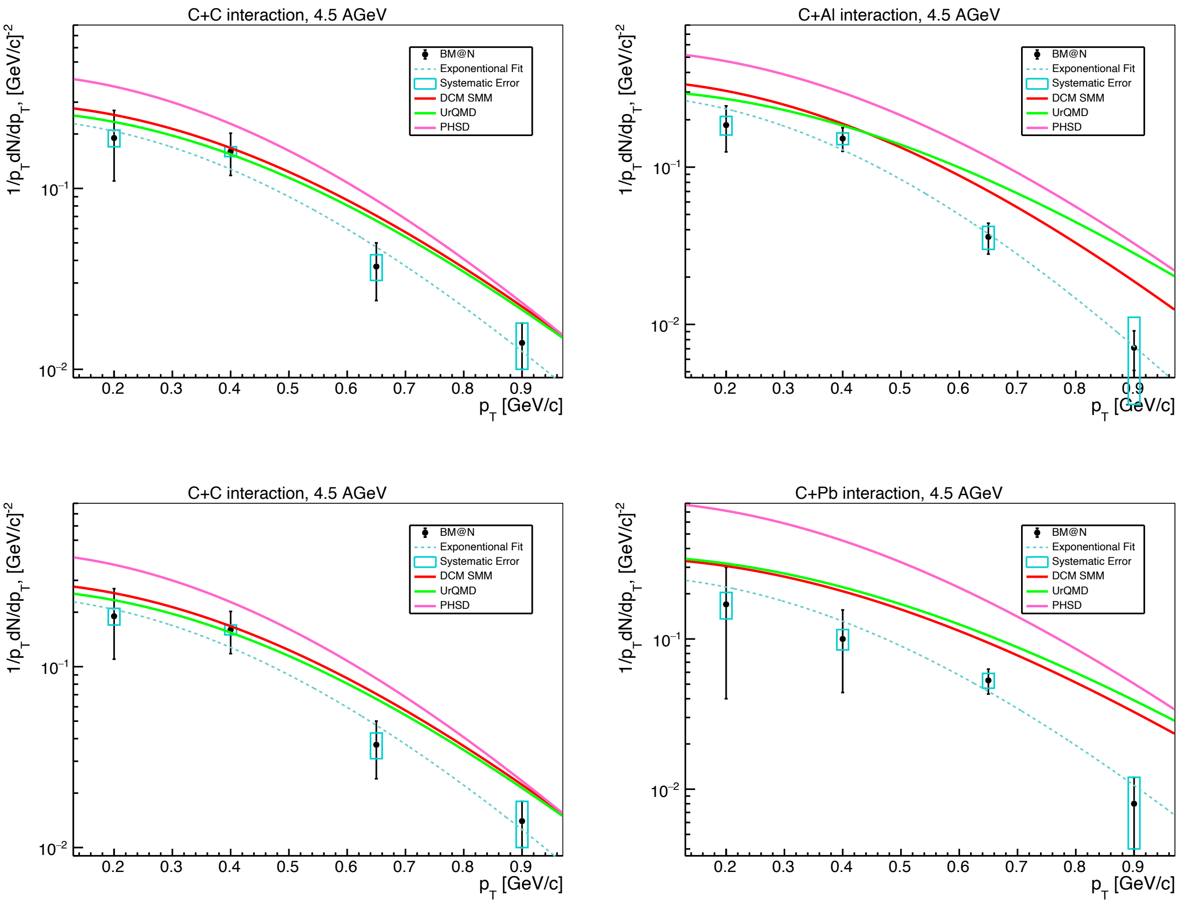

Figure 39. Invariant transverse momentum p_T spectra of Λ hyperons in minimum bias *C+C* (top left*)*, *C+Al* (top right)*, C+Cu* (bottom left), *C+Pb* (bottom right) interactions at 4.5 AGeV carbon beam energy. The error bars represent the statistical errors, the blue boxes show the systematic errors. The blue lines represent the results of the parameterization described in the text. The predictions of the DCM-SMM, UrQMD and PHSD models are shown as colored lines.

The fit results are consistent within the uncertainties with the predictions of the DCM-SMM, UrQMD and PHSD models. In general, the models considered describe the shape of the differential spectra in y and p_T, but predict more abundant yields of Λ hyperons than measured in the experiment. The predictions of DCM-SMM and UrQMD models are closer to the experimental data than the predictions of the PHSD model. The PHSD model predicts a stronger increase in Λ hyperon yield in the BM@N kinematic range with an increasing atomic weight of the target than the DCM-SMM and UrQMD models. This tendency is deduced from the rapidity spectra of Λ hyperons generated in the models which are shown in Fig. 40

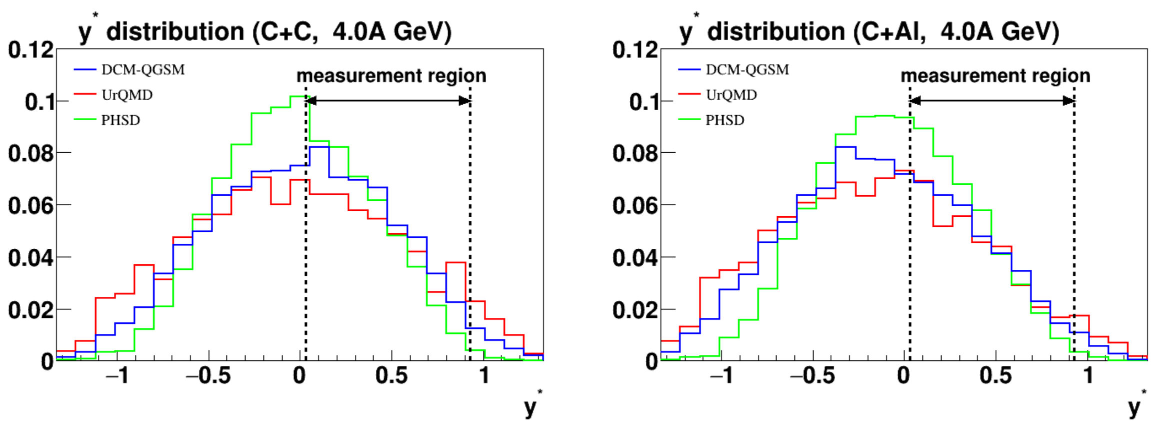

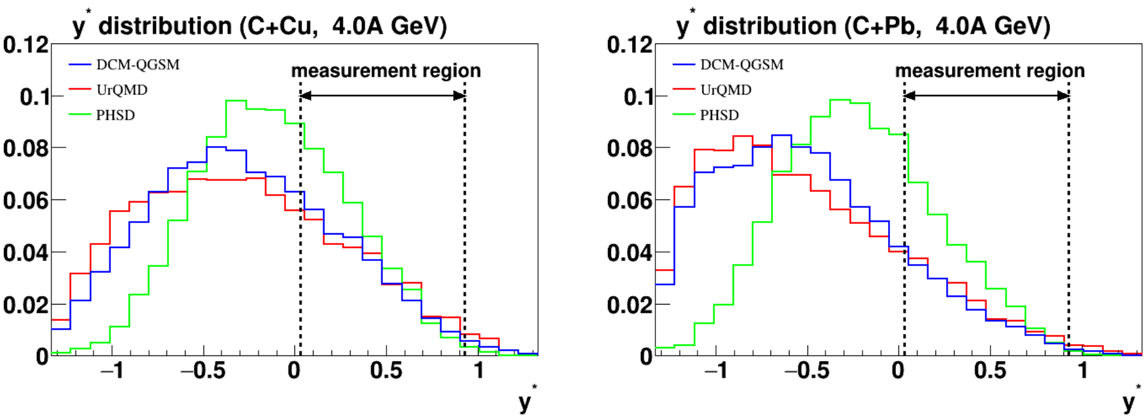

Figure 40. Rapidity spectra of *Λ* hyperons in minimum bias interactions of 4.0 AGeV carbon beam with *C, Al, Cu, Pb* targets, generated with the DCM-SMM (redraw), UrQMD and PHSD models. The BM@N measurement range in y is indicated.

Systematic uncertainties

The main sources of systematic uncertainty that contribute to the *Λ* hyperon yields can be characterized as follows:

1) Statistical fluctuations in Monte Carlo and experimental data

To evaluate the statistical fluctuations of the signal each bin of the reconstructed mass spectra distributions was smeared according to the Gaussian function, where the mean parameter corresponded to the bin value and sigma parameter corresponded to the statistical error. The varied signal distributions were fitted using Gaussian function and $\sigma_{N^{\Lambda}_{rec\,MC}}$ and $\sigma_{N^{\Lambda}_{rec\,DATA}}$ values were extracted from the fits. The systematic uncertainty from this source was estimated as:

$$\Delta Y_{\Lambda_{sys\_pseudo\_exp}} = Y_{\Lambda}\sqrt{\sigma_{N^{\Lambda}_{rec\,DATA}}{}^{2}/N^{\Lambda}_{rec_{DATA}}{}^{2} + \sigma_{N^{\Lambda}_{rec\,MC}}{}^{2}/N^{\Lambda}_{rec_{MC}}{}^{2}}, \tag{1.14}$$

where $N^{\Lambda}_{rec_{MC}}$ and $N^{\Lambda}_{rec_{DATA}}$ the values of the reconstructed *Λ* hyperons in the MC and experimental data, respectively.

2) Uncertainties due to selection cut criteria

To estimate the systematic error from this source a series of analyzes were performed with the different values of the "path" and "dca" selection parameters. The values variations of these parameters were performed within ±10% of the values used in the analysis. The maximal deviation of the calculated *Λ* yields values was 20% and the systematic uncertainty value was estimated as $\Delta Y_{\Lambda_{sys_{cut\_var}}} = 0.004$.

3) The total systematic error was calculated as:

$$\Delta Y_{\Lambda_{sys}} = \sqrt{\Delta Y_{\Lambda_{sys\_pseudo\_exp}}{}^{2} + \Delta Y_{\Lambda_{sys_{cut\_var}}}{}^{2}} \tag{1.15}$$

The systematic uncertainties are summarized in Tables 10 and 11.

Table 10. Total systematic uncertainty of the Λ yield for 4.0 AGeV

Target / Interval	*y*				Target / Interval	p_T			
	C sys%	***Al*** sys%	***Cu*** sys%	*Pb* sys%		***C*** sys%	***Al*** sys%	***Cu*** sys%	***Pb*** sys%
1.2 -1.45	17.6	7.8	11.9	8.5	0.1 - 0.3	20.0	10.2	10.6	-
1.45-1.65	27.3	8.7	8.5	10.4	0.3 - 0.5	17.6	7.9	9.2	
1.65-1.85	20.6	21.1	12.1	16.7	0.5 - 0.75	25.0	13.3	12.5	
1.85-2.1	33.3	44.4	16.3	29.4	0.75 - 1.05	50.0	30.8	30.8	
Normalization	4.9	3.8	3.0	3.0	Normalization	4.9	3.8	3.0	3.0

Table 11. Total systematic uncertainty of the Λ yield for 4.5 AGeV.

Target / Interval	*y*				Target / Interval	p_T			
	C, sys%	***Al,*** sys%	***Cu***, sys%	***Pb,*** sys%		***C***, sys%	***Al,*** sys%	***Cu,*** sys%	***Pb,*** sys%
1.2-1.45	16.7	11.9	6.8	15.7	0.1-0.3	18.8	13.5	7.9	21.0
1.45-1.65	23.1	9.0	4.9	12.8	0.3-0.5	11.4	8.3	6.9	9.4
1.65-1.85	37.5	19.0	10.3	11.7	0.5-0.75	25.3	17.4	9.8	11.8
1.85-2.1	25.0	26.7	12.9	33.3	0.75-1.05	33.3	33.3	36.1	28.5
Normalization	4.9	3.8	3.0	3.0	Normalization	4.9	3.8	3.0	3.0

Integrated yields and cross sections

The integrated Λ yields, cross sections and inverse slope parameters T_0 for *C +C, C +Al, C +Cu, C + Pb* interactions are summarized in Tables 12 and 13. The measured Λ yields within BM@N acceptance ($0.1<p_T<1.05$ GeV/*c* and $1.2 <y<2.1$) were extrapolated to the full kinematic range. The extrapolation factor values were calculated as the average predictions of the DCM-SMM and UrQMD models. The calculated Λ yields in full kinematic region and the extrapolating factor values are also presented in Tables 12, 13.

The Λ yields and production cross sections in *C+C* interactions can be compared with the previous results of the 23.2±2.5 mb [9] and 24±6 mb [10] measured in interactions of the carbon beam with the momentum of 4.2 GeV/*c* per nucleon (beam kinetic energy of 3.36 AGeV per nucleon) with the Propane Chamber experiment. On Fig. 41 the BM@N results for the Λ hyperon yields in *C + C* minimum bias interactions are compared with the results taken from the Propane Chamber experimental data analysis. In Table 14 yields and inclusive cross sections of Λ hyperon production in interactions of light and medium nucleus from the other experiments are presented for the comparison.

The BM@N results are compared with the predictions of the DCM-SMM, UrQMD and PHSD models (Fig. 41, 42 and Tab. 15). The tendency of the Λ hyperon yields to increase with increasing energy is observed. In general, the model predictions exceed the experimental data. PHSD model predicts higher full yields of the Λ hyperons than the other two models.

Table 12. Extrapolation factors to the full kinematic range, reconstruction efficiencies, Λ hyperon yields and cross sections for 4.0 AGeV data. The first error given is statistical, the second error is systematic.

4.0 AGeV	***C***	***Al***	***Cu***	***Pb***
DCM-SMM & URQMD extrap. factor (average)	2.49±0.18	3.01±0.13	4.0±0.06	6.72±0.44

Efficiency in 0.1<p_T<1.05 GeV/c, 1.2<y_{lab}<2.1	0.032 ± 0.001	0.026 ± 0.001	0.022± 0.001	0.016 ± 0.001
Yields in 0.1<p_T<1.05 GeV/c, 1.2<y_{lab}<2.1	0.023 ± 0.003 ± 0.005	0.032 ± 0.004 ± 0.006	0.030 ± 0.003 ± 0.005	low statistics
Yields in the full kin. range	0.057 ± 0.007 ±0.01	0.096 ± 0.01 ± 0.02	0.12 ± 0.01± 0.02	
Λ cross section in min. bias interact, mb	47.3 ± 5.8 ± 8.3	121.0 ± 15.1 ± 22.7	214.8 ± 21.5 ± 35.8	
Inverse slope parameter, MeV χ2/ndf	89 ±9± 17 1.83	99 ± 10 ±16 0.57	108 ± 11 ± 14 0.1	

Table 13. Extrapolation factors to the full kinematic range, reconstruction efficiencies, Λ hyperon yields and cross sections for 4.5 AGeV data. The first error given is statistical, the second error is systematic.

4.5 AGeV	***C***	***Al***	***Cu***	***Pb***
DCM-QGSM & URQMD extrap. factor (average)	2.34 ± 0.08	2.88 ± 0.16	3.76 ± 0.15	6.24 ± 0.14
Efficiency in 0.1<p_T<1.05 GeV/c, 1.2<y_{lab}<2.1	0.027 ± 0.0003	0.024 ± 0.0003	0.020 ± 0.0002	0.015± 0.0003
Yields in 0.1< p_T< 1.05 GeV/c, 1.2< y <2.1	0.027 ± 0.005 ± 0.006	0.025 ± 0.003± 0.005	0.037 ± 0.004 ± 0.006	0.033 ± 0.010 ± 0.010
Yields in the full kin. range	0.063 ± 0.012 ± 0.014	0.071 ± 0.009± 0.014	0.14 ± 0.02 ± 0.02	0.20 ± 0.06 ± 0.06
Λ cross section in min. bias interact., mb	52.5 ± 9.7 ± 11.6	90.7 ± 11.3 ± 18.1	249.0 ± 35.8 ± 40.3	633.2 ± 191.9 ± 191.9
Inverse slope parameter, MeV χ2/ndf	107 ± 17 ± 17 1.00	86 ± 8 ±17 0.77	91 ± 8 ±15 0.19	99 ± 17 ± 20 0.78

Table 14. Yields and inclusive cross sections of Λ hyperon production in interactions of light and medium nucleus.

Interacting nucleus / reference	**Beam momentum, kinetic energy (E_{kin})**	**Λ cross section, mb**	**Λ yield, $\cdot 10^{-2}$**
He_4+Li_6	4.5 GeV/c (3.66 AGeV)	5.9± 1.5	1.85 ± 0.5
*C+C, P*ropane Chamber	4.2 GeV/c (3.36 AGeV)	24 ± 4 [10]	2.89±0.72
*C+C, P*ropane Chamber	4.2 GeV/c (3.36 AGeV)	23.2±2.5 [9]	2.8 ± 0.3
p+p	4.95 GeV/c (4.1 AGeV)		2.3 ± 0.4
Ar+KCl, HADES	1.76 AGeV		3.93±0.14±0.15
Ar+KCl, FOPI	1.93 AGeV		3.9±0.14±0.08
Ni+Ni, FOPI, central 390 mb from 3.1 *b*	1.93 AGeV		$0.137{\pm}0.005{\pm}^{0.009}_{0.025}$

Ni+Cu, EOS, full *b*<8.9 fm / central *b*<2.4 fm	2.0 AGeV	112±24 / 20±3	
Ar+KCl, central *b*<2.4 fm	1.8 AGeV	7.6±2.2	

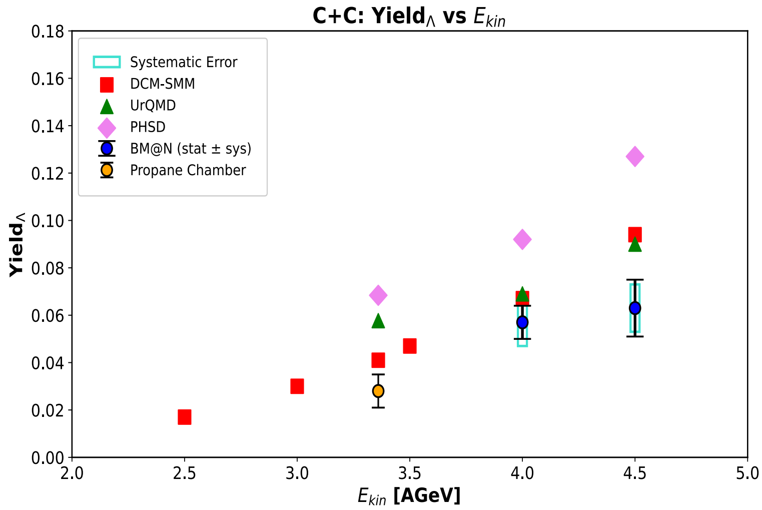

Figure 41. Energy dependence of *Λ* yields measured in different experiments. The error bars represent the statistical errors, the blue bands show the systematic errors. BM@N result is compared with data taken from another experiments [9], [10]. The predictions of the DCM-SMM, UrQMD and PHSD models are shown as colored lines.

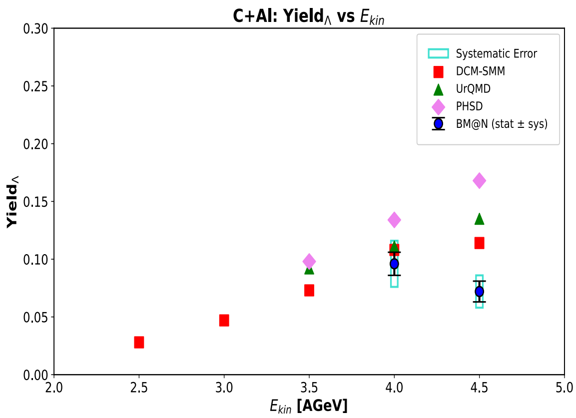

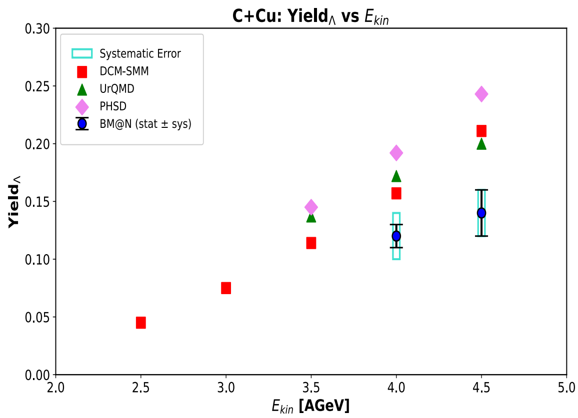

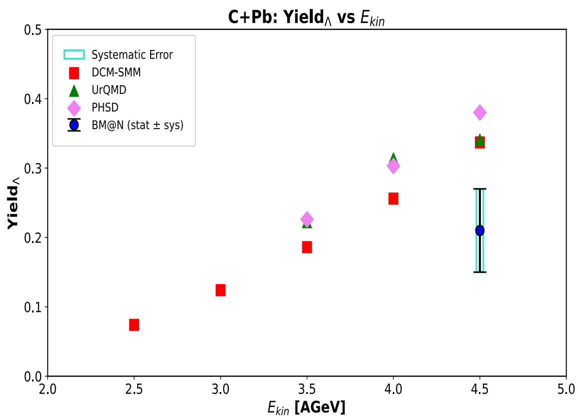

Figure 42. Energy dependence of *Λ* yields measured in BM@N experiment for the minimum bias interactions. The error bars represent the statistical errors, the blue bands show the systematic errors. The predictions of the DCM-SMM, UrQMD and PHSD models are shown as colored lines.

Table 15. *Λ* hyperon yields and their values normalized to the number of nucleons-participants. The first error is statistical, the second error is systematic. Predictions of the DCM-QGSM, UrQMD and PHSD models are shown for *C+A* interactions at different beam energies.

C+C	**4.5 AGeV**	**4.0 AGeV**	**3.5 AGeV**	**3.0 AGeV**	**2.5 AGeV**
BM@N yield Yield/N_{part}	0.063 ± 0.012 ± 0.014 0.007 ±0.0013 ±0.0016	0.057 ± 0.007 ±0.01 0.0063 ±0.0008 ±0.0011			
DCM-SMM N_{part} Yield/N_{part}	0.094 9 0.0104	0.067 9 0.0074	0.047 9 0.0052	0.03 9 0.0033	0.005 9 0.0006
UrQMD yield N_{part} Yield/N_{part}	0.093 7.2 0.0129	0.073 7.2 0.0101	0.058 7.2 0.0081		
PHSD yield N_{part} Yield/N_{part}	0.117 8.4 0.0139	0.09 8.4 0.0107	0.068 8.4 0.0081		
Other Experiments			0.0289±0.0072 (3.36AGeV) 0.028±0.003 (3.36 AGeV) Propane Chamber		

C+Al	**4.5 AGeV**	**4.0 AGeV**	**3.5 AGeV**	**3.0 AGeV**	**2.5 AGeV**
BM@N yield Yield/N_{part}	0.071 ± 0.009± 0.014 0.0053 ±0.0007 ±0.001	0.096 ± 0.01 ± 0.02 0.0071±0.0007 ±0.0015			
DCM-SMM N_{part} Yield/ N_{part}	0.14 13.4 0.0104	0.11 13.4 0.0082	0.073 13.4 0.0054	0.047 13.4 0.0035	0.028 13.4 0.0021
UrQMD yield N_{part} Yield / N_{part}	0.141 11.4 0.0124	0.114 11.4 0.01	0.092 11.4 0.0081		
PHSD yield N_{part} Yield/ N_{part}	0.169 11.9 0.0142	0.134 11.9 0.0112	0.098 11.9 0.0082		
C+Cu	**4.5 AGeV**	**4.0 AGeV**	**3.5 AGeV**	**3.0 AGeV**	**2.5 AGeV**
BM@N yield Yield/N_{part}	0.14 ± 0.02 ± 0.02 0.0061±0.0009±0.0009	0.12 ± 0.01± 0.02 0.0052±0.0004±0.0009			
DCM-SMM N_{part} Yield/N_{part}	0.211 23.0 0.0092	0.157 23.0 0.0068	0.114 23.0 0.005	0.075 23.0 0.0033	0.006 23.0 0.0003
UrQMD yield N_{part} Yield / N_{part}	0.211 19.3 0.0109	0.159 19.3 0.0082	0.137 19.3 0.0071		
PHSD yield N_{part} Yield / N_{part}	0.243 17.3 0.014	0.191 17.3 0.011	0.145 17.3 0.0084		
C+Pb	**4.5 AGeV**	**4.0 AGeV**	**3.5 AGeV**	**3.0 AGeV**	**2.5 AGeV**

BM@N yield Yield/N_{part}	0.20 ± 0.06 ± 0.06 0.004±0.0012±0.0012	low ststistic			
DCM-SMM N_{part} Yield / N_{part}	0.337 50.5 0.0067	0.256 50.5 0.0051	0.186 50.5 0.0037	0.124 50.5 0.0025	0.074 50.5 0.0015
UrQMD yield N_{part} Yield/ N_{part}	0.35 50.0 0.007	0.295 50.0 0.0059	0.221 50.0 0.0042		
PHSD yield N_{part} Yield/ N_{part}	0.38 30.8 0.0123	0.303 30.8 0.0098	0.226 30.8 0.0073		

The calculated *Λ* hyperon yields in full kinematic region for the *C +C* collisions were compared with a parameterization model developed for proton-proton (*p*+*p*) interactions and scaled to the *C + C* system.

The parameterization model is based on the Lund String Model (LSM) [11] and is expressed as:

$$\langle n_{pp} \rangle = a(x-1)^b x^{-c}, \quad (1.16)$$

where: $x = s/s_0$ is the square of the center-of-mass energy;
s_0 – is the square of the production threshold;
a, b, c – are the fit parameters from [12].

Since *C*+*C* includes not only *p*+*p* but also *p*+*n* and *n*+*n* interactions, and near threshold of *Λ* yield are about 25% lower in n+n and n+p compared to p+p [13], the isospin correction factor was calculated as:

$$k_{iso} = f_{pp} \cdot \alpha + \left(f_{np} + f_{pn} + f_{nn}\right) \cdot \beta, \quad (1.17)$$

with $\alpha = 1.0$ for *p*+*p* and $\beta = 0.75$ for *n*+*n*, *n*+*p*, and *p*+*n* collisions. The fractions f_{ij} are determined by the composition of nucleons in the colliding carbon nuclei. The total yield $\langle n_\Lambda \rangle$ for *C*+*C* was scaled as:

$$\langle n_\Lambda \rangle = \langle n_{pp} \rangle \cdot k_{iso} \cdot N_{part}, \quad (1.18)$$

where: N_{part} in the number of the participating nucleons;
k_{iso} – is the isospin correction factor.

The BM@N results for the *Λ* yields in the *C + C* collisions at 4.0AGeV and 4.5 AGeV are in good agreement with the scaled $p + p$ parameterization model (Fig. 43). The parameterization provides a reliable basis for the estimation of *Λ* hyperon production in carbon-carbon interactions. The agreement with the BM@N experimental data supports its applicability for light-symmetric systems. In addition, the number of participating nucleons N_{part} used in the scaling was taken from the DCM-SMM [14] model and it was evaluated according to existing measurements from the Propane Chamber experiment.

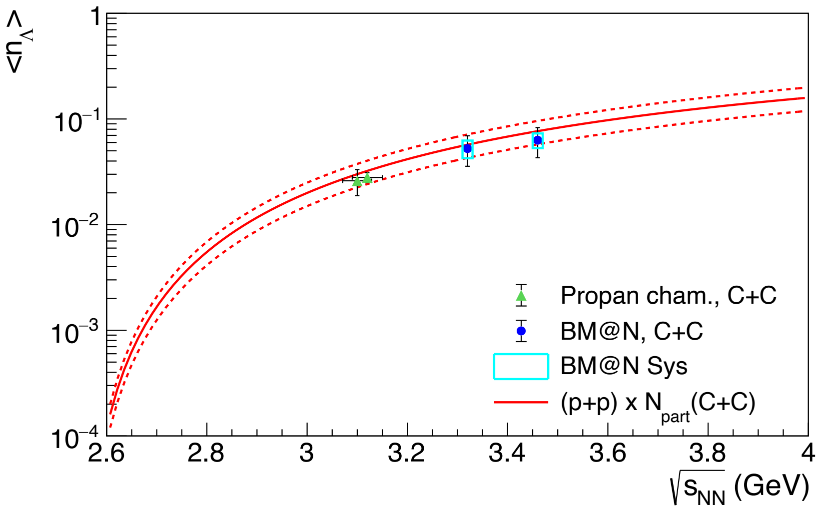

Figure 43. The integrated yield of Λ hyperons in $C + C$ collisions as a function of $\sqrt{s_{NN}}$. BM@N experimental data are compared with a parameterization model based on p+p collisions scaled to the N_{part}= 9. Dashed red lines indicate the uncertainties in the predicted excitation function (about 25%).

To compare yields of particle production in nucleus-nucleus interactions, they are usually normalized to the number of nucleon participants. For the DCM-SMM, UrQMD, PHSD models the number of participants in the reactions *C+C, C+Al, C+Cu, C+Pb* was calculated (Tab. 15). For the both energies 4.0 AGeV and 4.5 AGeV the obtained N_{part} values are the same.

The integrated Λ hyperon yields for each model were normalized to the corresponding number of participants N_{part}. The experimental data were normalized to the N_{part} values obtained for the DCM-SMM model. The ratios of the Λ hyperon yields to the number of nucleons participants measured by BM@N are given in Table 15. Comparison of experimental data with the predictions of the DCM-SMM, UrQMD and PHSD models for 4.0 AGeV and 4.5 AGeV carbon nucleus interactions is shown in Fig. 44. There is a tendency that the measured ratios are smoothly decreasing for heavier target nuclei. This tendency is also predicted by the models.

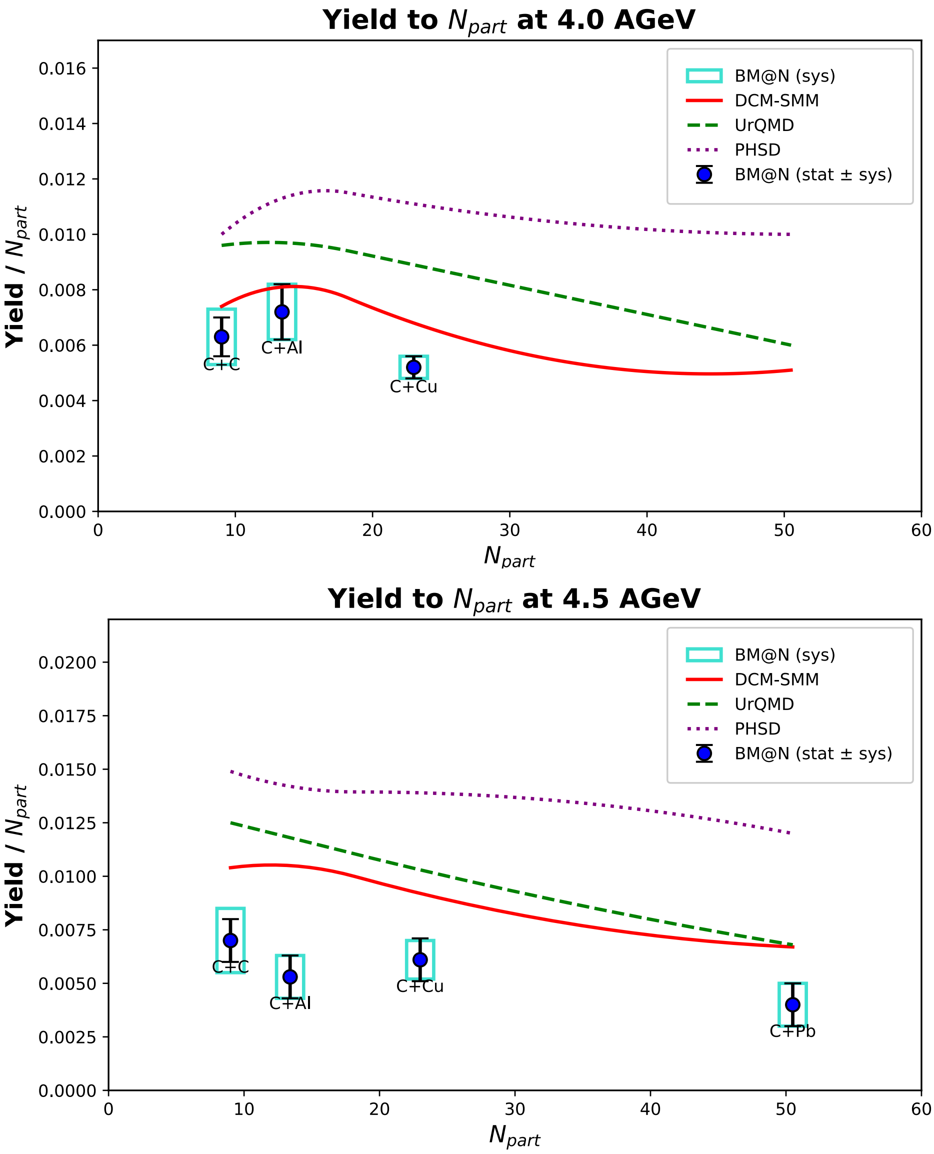

Figure 44. Ratios of the Λ hyperon yields to the number of nucleons-participants measured by BM@N in minimum bias carbon-nucleus interactions at 4.0 AGeV (top) and 4.5 AGeV (bottom). Error bars show statistical uncertainties, while blue rectangles indicate systematic errors. The predictions of the DCM-SMM, UrQMD and PHSD models are shown in colored lines

Summary

The production of Λ hyperons in the interactions of the carbon beam with the *C, Al, Cu, Pb* targets was measured with the BM@N detector. The physical results of the BM@N experiment are presented on the Λ hyperon yields and cross sections in minimum bias carbon nucleus interactions at beam kinetic energies of 4.0 AGeV and 4.5 AGeV. The results are compared with DCM-SMM, UrQMD, PHSD models of nucleus-nucleus interactions and with the results of other experiments studied carbon-carbon interactions at lower energies.

The Λ hyperon cross sections were evaluated to be (47.3 ± 5.8 mb) and (52.5 ± 9.7 mb) for carbon-carbon collisions at energies of 4.0 AGeV and 4.5 AGeV, respectively. These values are about twice those measured in the propane chamber at energies of 3.36 AGeV (24 ± 6 mb and 23.2±2.5), showing a general increase in cross section with increasing energy. The cross sections and yields of Λ hyperons in the $C + Al$, $C + Cu$, and $C + Pb$ (only for 4.5 AGeV) collisions are presented in Tables 12 and 13 for both beam energies and in Figs. 41-42. Due to the limited kinematic conditions and set of target nuclei, it is not possible at this time to make a direct comparison with other experiments, as similar data are not available.

The BM@N results for Λ production in $C + C$ collisions at 4.0 AGeV and 4.5 AGeV show good agreement with a proton-proton based parameterization model scaled to the carbon-carbon system. The scaling includes into account the number of participants involved in reaction estimated by the DCM-SMM model as well as isospin effects. This comparison is shown in Figure 43.

In the studied energy ranges the differences between the experimental temperature measurements are not large within the uncertainty values. The temperature increases with increasing atomic number of the target nucleus within the uncertainty limits. For more accurate determination of the temperature dependence it is important to continue such experimental studies.

Acknowledgments

The BM@N Collaboration gratefully acknowledges the support of BM@N DAQ Cluster Team for providing the necessary resources and facilities that contributed to this research.

Bibliography

[1]https://bmn-wiki.jinr.int/bin/download/Doc/4.%20Documents/4.6%20Internal%20Notes/BM%40N%20GEM%20tracker%20characteristics%2C%20BM%40N%202015-01%20SIM-001/WebHome/bmnnote_2015_01.pdf?rev=1.1

[2] BM@N Conceptual Design Report: http://nica.jinr.ru/files/BM@N/BMN_CDR.pdf

[3] D.Baranov et al., First Results from BM@N Technical Run with Deuteron Beam, Phys. Part. Nucl. Lett. 15, no. 2, 148 (2018)

[4] V. Akishina and I. Kisel. Time-based cellular automaton track finder for the CBM experiment - 2015. J. Phys.: Conf. Ser. 599, 012024

[5] S. Gorbunov and I. Kisel. Reconstruction of decayed particles based on the Kalman filter - 2007. CBM-SOFTnote—003

[6] K. Alishina, Yu. Yu. Stepanenko, A. Y. Khukhaeva. GEM residuals correction in Monte-Carlo simulation for the Run-6 of the BM@N experiment Physics of Particles and Nuclei Letters, 2022, Vol. 19, No. 5, pp. 485–488. © Pleiades Publishing, Ltd., 2022. ISSN 1547-477.

[7] Study of Λ-hyperon production in collisions of the heavy ions with solid targets in the BM@N experiment. K. Alishina, Yu. Yu. Stepanenko. Physics of Particles and Nuclei Letters, 2024, Vol. 21, No. 4, pp. 683–686. © Pleiades Publishing, Ltd., 2024. ISSN 1547-4771.

[8] H.Angelov et al., P1-80-473, JINR, Dubna

[9] D.Armutlijsky et al., Report No, P1-85-220, JINR, Dubna

[10] S.Arakelian et al., Report No, P1-83-354, JINR, Dubna

[11] W. Cassing and E. L. Bratkovskaya, “Hadronic and electromagnetic probes of hot and dense nuclear matter,” Phys. Rep. 308, 65 (1999).

[12] V.Kolesnikov, V. Kireyeu, V. Lenivenko, A. Mudrokh, K. Shtejer, D. Zinchenko, and E. Bratkovskaya, A New Review of Excitation Functions of Hadron Production in pp Collisions in the NICA Energy Range, PEPAN Letters (2020), Vol. 17, №2, pp. 142-153.

[13] V. Kireyeu, I. Grishmanovskii, V. Kolesnikov, V. Voronyuk, E. Bratkovskaya, Hadron production in elementary nucleon–nucleon reactions from low to ultra-relativistic energies, Eur. Phys. J. A (2020) 56: 223

[14] M. Baznat, A. Botvina, G. Musulmanbekov, V. Toneev, V. Zhezher, Phys.Part.Nucl.Lett. 17 (2020) no.3; arXiv: 1912.09277v.